Letters in Drug Design & Discovery 23 (2026) 100402

Contents lists available at ScienceDirect

Letters in Drug Design & Discovery

journal homepage: www.keaipublishing.com/en/journals/lddd/

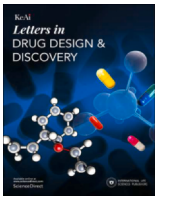

Synthesis of new metacetamol azo derivatives and assessment of their antibacterial and pharmacological potential

Kai Wei Yeo[a], Nor Hisam Zamakshshari[a], Ainaa Nadiah Abd Halim[a,*], Wan Sharifatun Handayani Wan Zullkiplee[b], Aina Syakirah Mohammad Hussin[a], D.'artaqnand Daniel[a], Halvy Hilary David[a], Nur Izzah Haziyah Ishak[a], Matherine Sadiah Mathew[a], Nur Alia Syahilda Zikri[a], Davlye Noissy Diosing[a], Sharon Hui Jiun Leong[a]

[a] Faculty of Resource Science and Technology, Universiti Malaysia Sarawak, Kota Samarahan, Sarawak 94300, Malaysia
[b] Centre for Pre-University Studies, Universiti Malaysia Sarawak, Kota Samarahan, Sarawak 94300, Malaysia

ARTICLE INFO

Keywords:
3-hydroxyacetanilide
3-acetaminophen
FtsA enzyme
Diazocoupling
ADME

ABSTRACT

Background: Metacetamol, a regioisomer of paracetamol known for its significantly lower toxicity, remains largely underexplored in medicinal chemistry despite its potential as a safer therapeutic scaffold. While paracetamol can cause hepatotoxicity through the accumulation of toxic metabolites, metacetamol presents an advantageous starting point for derivatisation and developing new pharmacological agents.

Objective: This study aims to synthesise new metacetamol azo derivatives **1–18** and perform structural elucidation with FTIR and NMR spectroscopies. The research further evaluates their antibacterial efficacy through both *in vitro* assays and *in silico* modelling.

Methods: The compounds were produced *via* a diazocoupling reaction between substituted anilines and metacetamol. Antibacterial potential against *Staphylococcus aureus* and *Escherichia coli* was pre-screened using the Kirby-Bauer disc diffusion, followed by the turbidimetric kinetic method for Minimum Inhibitory Concentrations (MIC) determination. Molecular docking was performed against the FtsA enzyme to investigate the mechanism of action, while SwissADME predicted druglikeliness and pharmacokinetic properties.

Result: Metacetamol azo **1–18** were successfully synthesised with yields ranging from 32% to 95%. Most derivatives exhibited notable antibacterial inhibition compared to the parent metacetamol, which showed no activity. Specifically, compound **2 *(m-F)*** demonstrated the highest activity against *E. coli* (MIC = 147.47 ppm), comparable to the reference drug, ampicillin (MIC = 118.14 ppm). All derivatives were found to comply with Lipinski's Rule of Five, suggesting high oral bioavailability and favourable GI absorption.

Discussion: The enhanced potency of compound ***2 (m-F)*** is attributed to the high electronegativity, specific *meta*-positional effect and small atomic size of the fluorine atom. These factors minimise steric hindrance while strengthening the C-F bond against metabolic transformation. Molecular docking reveals that ***2 (m-F)*** establishes stable hydrogen bonds with key residues of LYS17 and LYS254 in the FtsA enzyme, potentially inhibiting bacterial cell division. Furthermore,

Peer review under responsibility of The Editorial Board of Letters in Drug Design & Discovery.
* Corresponding author.
E-mail address: ahanadiah@unimas.my (A.N. Abd Halim).

https://doi.org/10.1016/j.lddd.2026.100402
Received 13 January 2026; Received in revised form 14 April 2026; Accepted 16 April 2026
Available online 22 April 2026

the azo linker improves molecular conjugation and binding affinity, while the secondary phenyl ring facilitates critical interactions with bacterial proteins through π-π stacking and hydrophobic forces.

Conclusion: Collectively, the strategic incorporation of an azo linker into metacetamol scaffold significantly elevates antibacterial activity while preserving desirable pharmacokinetic characteristics. These findings provide a promising starting point for optimising metacetamol-based agents as potential therapeutic candidates.

1. Introduction

The metacetamol, also known as 3-acetamidophenol, 3-acetaminophen or 3-hydroxyacetanilide, is a regioisomer of paracetamol that has been overlooked in derivatisation or medicinal chemistry efforts. In contrast, paracetamol is a prominent over-the-counter analgesic, antipyretic and a promising anti-arthritic drug [1,2]. However, paracetamol has evidence to cause worrying side effects such as acute liver failure and hepatotoxicity even at therapeutic dosage [3,4]. The minor paracetamol component that cannot be excreted by the kidney is oxidised by the cytochrome P450, leading to accumulation of *N*-acetyl-*p*-benzoquinone imine (NAPQI) than glutathione detoxification capacity, causing a series of reactions such as inducing oxidative stress, mitochondrial dysfunction and necrotic cell death [5,6]. Consequently, the attention of researchers has been slowly shifted towards metacetamol due to its lower toxicity than paracetamol, positioning it as an underexplored yet promising scaffold for the development of safer therapeutic functions [7].

There have been a few recent studies reported on metacetamol derivatives for biological capabilities. Significant discovery reported with levofloxacin, as a well-known antibacterial agent that is often prescribed to patients, was able to form a co-crystal with metacetamol, which was highlighted to have better physicochemical and pharmacological properties as compared to paracetamol [8]. In the subsequent year, Joolakanti *et al.* (2021) reported that the incorporation of metacetamol with 1,2,3-triazole derivatives has shown commendable antibacterial, antioxidant and anti-inflammatory activities. Meanwhile, a study done by Şenkardeş *et al.* (2023)[9] yielded positive results for synthesising dual functional drugs, antibacterial and anticancer agents, by using metacetamol as a starting material.

The current strategy for effective drug design and development directed towards the fusion of two or more pharmacophores elevates the binding affinity of drugs, enhances the biological activities through synergistic actions and reduces the drug resistance [10,11]. Based on the aforementioned hypotheses, the azo linker (-N = N-) is the essential pharmacophore that enhances conjugation and modulates the physicochemical properties of the compound, which has been incorporated into the drug target molecules for a wide range of biological activities [12]. Several examples of marketed drugs with an azo linker are prontosil antibacterial drugs [13], basalazide [14], sulfasalazine [15,16], olasalazine [17], and phenazopyridine [18]. The promising activities of the azo moiety are achieved by involving several mechanisms, such as suppression of the proliferation rate of the pathogen, reducing the synthesis of DNA, RNA and protein production [19].

Hence, in this study, an azo linker was incorporated into compounds **1–18** from the diazonium coupling reaction of electron-withdrawing and electron-donating substituted aniline with metacetamol. The different substituents at different positions of aniline would influence the receptor selectivity [20]. In addition, previous literature has reported that the presence of electron-withdrawing groups leading to electron deficiency of compounds would strengthen the interaction with the bacterial sites, enhancing the biological activity [21]. Whereas, the existence of an electron-donating group increases the lipophilicity of the compounds, aiding the penetration of the cell membrane [22]. Upon obtaining the metacetamol azo **1–18**, their antibacterial activity was evaluated *via* the Kirby-Bauer disc diffusion for initial screening, followed by minimum inhibitory concentration (MIC) determination using the Turbidimetric Kinetic method against Gram-positive bacteria (*Staphylococcus aureus*, ATCC 25923) and Gram-negative bacteria (*Escherichia coli*, ATCC 25922), with ampicillin as a reference drug. Subsequently, molecular docking analysis was carried out to gain insight into the interaction of the compounds with targeted proteins. The physicochemical and pharmacokinetic properties of the compounds were also studied by employing the SwissADME online tool, as the substituent of the compound could affect the absorption, distribution, metabolism and excretion (ADME) properties of the compound and its druglikeness properties [23].

2. Materials and methods

2.1. Measurement and reagents

All the reagents and solvents were purchased from Merck (Darmstadt, Germany) sources through a local supplier and used without further purification. Melting points of the compounds were analysed using an open tube capillary Stuart SMP3 (Stone, Staffordshire, United Kingdom). Thermo Fisher ScientificTM Flash 2000 Analysers (Waltham, Massachusetts, United States) were used for the elementary analysis CHNS. The Fourier Transform Infrared Spectroscopy (FTIR) was deployed to identify the presence of functional groups via Perkin Elmer Thermo Fisher Scientific Smart Omni Transmission Nicolet 1605 (Madison, USA) spectrophotometer. The compounds were dissolved in DMSO-d6 before being scanned with JOEL ECA 500 (Kobe, Japan) for ^{1}H at 500 MHz and ^{13}C at 125 MHz, and chemical shifts were recorded in δ ppm. A Shimadzu UV-visible spectrophotometer (UV-1900i) (Negeri Sembilan, Malaysia) was used to perform optical measurements.

2.2. Synthesis of metacetamol azo derivatives (1 – 18)

Aniline derivatives (2 mmol) were dissolved in the mixture of distilled water (10 mL) and hydrochloric acid (6 mL, 3 M) before being cooled to a low temperature (0–5 °C). Sodium nitrite (2 mmol) dissolved in 10 mL of distilled water was added dropwise to the aniline derivatives to form a diazonium salt. The mixture was monitored closely by using potassium iodide-starch paper. Once the KI paper turned blue, indicating formation of diazonium salt, metacetamol (2 mmol) under alkaline conditions (pH 9–10) was added slowly into the solution [24]. The mixture was stirred for 15 min, and reaction completion was monitored by thin-layer chromatography (TLC) with a mobile phase of hexane: ethyl acetate (2:1) ratio. The precipitate obtained was filtered and rinsed with cold water and purified by recrystallisation in methanol and water (1:10) solutions.

(E)-N-(2-((2-fluorophenyl)diazenyl)-5-hydroxyphenyl)acetamide (1). ***o*-Fluoroaniline** (0.222 g, 2 mmol). **Yield** (0.404 g, 74%) as a yellow solid, **m.p.** 245℃ - 246℃. (**Found**: C, 61.40; H, 4.46; N, 15.34. $C_{14}H_{12}FN_3O_2$ Requires C, 61.53; H, 4.43; N, 15.38%). ν_{max} (cm^{-1}) 3113 (OH), 1661 (C═O), 1606 (Ar-C), 1551 (N = N), 1307 (C-N). **^{1}H NMR** (500 MHz, DMSO-d6), δH (ppm): 2.19 (3 H, s, CH_3), 6.63 (2 H, dd, J = 11.5 Hz, J = 2 Hz, Ar-H), 7.34 (1 H, t, J = 8 Hz, Ar-H), 7.45 (1 H, t, J = 11.5 Hz, Ar-H), 7.69 (2 H, d, J = 10 Hz, Ar-H), 7.91 (1 H, s, Ar-H), 10.54 (1 H, s, NH), 10.58 (1 H, s, OH). **^{13}C NMR** (125 MHz, DMSO-d6), δc (ppm): 25.1 (CH_3), 106.8, 111.6, 117.0, 117.8, 122.4, 124.9, 132.2, 133.9, 138.4 (C-N = N-), 138.8 (C-NH), 157.9 (C-N = N-), 159.9 (C-OH), 162.4 (C-F), 169.1 (C═O).

(E)-N-(2-((3-fluorophenyl)diazenyl)-5-hydroxyphenyl)acetamide (2). ***m*-Fluoroaniline** (0.222 g, 2 mmol). **Yield** (0.453 g, 83%) as a yellow solid, **m.p.** 235℃ - 236℃. (**Found**: C, 61.68; H, 4.39; N, 15.09. $C_{14}H_{12}FN_3O_2$ Requires C, 61.53; H, 4.43; N, 15.38%). ν_{max} (cm^{-1}) 3378 (NH), 3111 (OH), 1667 (C═O), 1593 (Ar-C), 1536 (N = N), 1318 (C-N). **^{1}H NMR** (500 MHz, DMSO-d6), δH (ppm): 2.18 (3 H, s, CH_3), 6.62 (1 H, dd, J = 11.5 Hz, J = 3 Hz, Ar-H), 7.27 (1 H, t, Ar- H), 7.56 (1 H, m, Ar-H), 7.66 (2 H, d, J = 9.5 Hz, Ar-H), 7.73 (1 H, d, J = 7.5 Hz, Ar-H), 7.84 (1 H, s, Ar-H), 10.12 (1 H, s, NH). **^{13}C NMR** (125 MHz, DMSO-d6), δc (ppm): 24.5 (CH_3), 107.2, 107.4, 111.7, 117.0, 120.4, 131.9, 133.9, 138.9 (C-N = N-), 154.0 (C-NH), 161.9 (C-N = N-), 162.4 (C-OH), 163.9 (C-F), 169.2 (C═O).

(E)-N-(2-((4-fluorophenyl)diazenyl)-5-hydroxyphenyl)acetamide (3). ***p*-Fluoroaniline** (0.222 g, 2 mmol). **Yield** (0.432 g, 79%) as a yellow solid, **m.p.** 228℃ - 229℃. (**Found**: C, 61.31; H, 4.31; N, 15.55. $C_{14}H_{12}FN_3O_2$ Requires C, 61.53; H, 4.43; N, 15.38%). ν_{max} (cm^{-1}) 3371 (NH), 3121 (OH), 1659 (C═O), 1605 (Ar-C), 1542 (N = N), 1317 (C-N). **^{1}H NMR** (500 MHz, DMSO-d6), δH (ppm): 2.19 (3 H, s, CH_3), 6.58 (1 H, dd, J = 11.5 Hz, J = 3 Hz, Ar-H), 7.37 (2 H, t, Ar-H), 7.66 (1 H, dd, J = 14 Hz, J = 5 Hz, Ar-H), 7.85 (1 H, s, J = 9 Hz, Ar-H), 7.98 (2 H, m, Ar-H), 10.18 (1 H, s, NH). **^{13}C NMR** (125 MHz, DMSO-d6), δc (ppm): 24.6 (CH_3), 107.3, 111.8, 116.0, 119.8, 124.6, 124.7, 133.3, 138.8 (C-N = N-), 149.0 (C-NH), 162.1 (C-N = N-), 162.9 (C-OH), 164.0 (C-F), 168.9 (C═O).

(*E*)-*N*-(2-((2-chlorophenyl)diazenyl)-5-hydroxyphenyl)acetamide (4). ***o*-Chloroaniline** (0.255 mL, 2 mmol). **Yield** (0.458 g, 79%) as orange, **m.p.** 246℃ - 247℃. (**Found**: C, 57.66; H, 4.15; N, 14.69. $C_{14}H_{12}ClN_3O_2$ Requires C, 58.04; H, 4.17; N, 14.50%). ***ν*max** (cm^{-1}) 3443 (NH), 3102 (OH), 1663 (C═O), 1607 (Ar-C), 1530 (N = N), 1315 (C-N). **^{1}H NMR** (500 MHz, DMSO-d6), δH (ppm): 2.20 (3 H, s, CH_3), 6.68 (1 H, dd, J = 11.5 Hz, J = 3.00 Hz, Ar-H), 7.48 (2 H, m, Ar-H), 7.66 (1 H, d, J = 7.5 Hz, Ar-H), 7.75 (1 H, d, J = 9 Hz, Ar-H), 7.87 (1 H, dd, J = 10 Hz, J = 2.5 Hz, Ar-H), 7.98 (1 H, d, J = 3 Hz, Ar-H), 10.73 (1 H, s, NH). **^{13}C NMR** (125 MHz, DMSO-d6), δc (ppm): 24.9 (CH_3), 106.8, 111.7, 118.0, 125.0, 128.5, 130.4, 131.5, 132.9 (C-Cl), 133.7 (C-N = N-), 137.8 (C-NH), 147.9 (C-N = N-), 162.7 (C-OH), 169.3 (C═O).

(*E*)-*N*-(2-((2-chlorophenyl)diazenyl)-5-hydroxyphenyl)acetamide (5). ***m*-Chloroaniline** (0.255 mL, 2 mmol). **Yield** (0.429 g, 74%) as reddish yellow, **m.p,** 240℃ - 241℃. (**Found**: C, 57.92; H, 4.39; N, 14.84. $C_{14}H_{12}ClN_3O_2$ Requires C, 58.04; H, 4.17; N, 14.50%). ***ν*max** (cm^{-1}) 3378 (NH), 1650 (C═O), 1612 (Ar-C), 1546 (N = N), 1375 (C-N). **^{1}H NMR** (500 MHz, DMSO-d6), δH (ppm): 2.21 (3 H, s, CH_3), 6.62 (1 H, dd, J = 9 Hz, J = 2.5 Hz, Ar-H), 7.54 (1 H, d, J = 7 Hz, Ar-H), 7.59 (1 H, t, J = 8 Hz, Ar-H), 7.68 (1 H, d, J = 9 Hz, Ar-H), 7.89 (2 H, d, J = 9 Hz, Ar-H), 8.00 (1 H, s, Ar-H), 10.19 (1 H, s, NH), 10.56 (1 H, s, OH). **^{13}C NMR** (125 MHz, DMSO-d6), δc (ppm): 24.6 (CH_3), 107.3, 111.6, 119.5, 120.9, 122.8, 129.8, 130.9, 133.8 (C-Cl), 134.0 (C-N = N-), 139.3 (C-NH), 153.2 (C-N = N-), 162.5 (C-OH), 169.0 (C═O).

(*E*)-*N*-(2-((4-chlorophenyl)diazenyl)-5-hydroxyphenyl)acetamide (6). ***p*-Chloroaniline** (0.255 g, 2 mmol). **Yield** (0.440 g, 76%) as golden yellow, **m.p.** 243℃ - 244℃. (**Found**: C, 58.27; H, 4.38; N, 14.25. $C_{14}H_{12}ClN_3O_2$ Requires C, 58.04; H, 4.17; N, 14.50%). ***ν*max** (cm^{-1}) 3458 (NH), 3109 (OH), 1664 (C═O), 1607 (Ar-C), 1545 (N = N), 1315 (C-N). **^{1}H NMR** (500 MHz, DMSO-d6), δH (ppm): 2.20 (3 H, s, CH_3), 6.62 (1 H, d, J = 9.00 Hz, Ar-H), 7.61 (2 H, d, J = 6.5 Hz, Ar-H), 7.67 (1 H, d, J = 9.00 Hz, Ar-H), 7.89 (1 H, s, Ar-H), 7.97 (2 H, d, J = 6.00 Hz, Ar-H), 10.16 (1 H, s, NH), 10.53 (1 H, s, OH). **^{13}C NMR** (125 MHz, DMSO-d6), δc (ppm): 24.6 (CH_3), 107.2, 111.6, 119.5, 124.2, 129.3, 133.7 (C-Cl), 134.7 (C-N = N-), 139.0 (C-NH), 150.8 (C-N = N-), 162.2 (C-OH), 168.9 (C═O).

(E)-N-(2((2-bromophenyl)diazenyl)-5-hydroxyphenyl)acetamide (7). ***o*-Bromoaniline** (0.344 g, 2 mmol). **Yield** (0.301 g, 45%) as yellow solid. **m.p.** 244°C - 245°C. (**Found**: C, 50.21; H, 3.68; N, 12.59. $C_{14}H_{12}BrN_3O_2$ Requires C, 50.32; H, 3.62; N, 12.57%). ***ν*max** (cm^{-1}) 3437 (NH), 3089 (OH), 1661 (C═O), 1604 (Ar-C), 1518 (N = N), 1313 (C-N). **^{1}H NMR** (500 MHz, DMSO-d6), δH (ppm): 2.22 (3 H, s, CH_3), 6.66 (1 H, dd, J = 9 Hz, J = 2.5 Hz, Ar-H), 7.40 (1 H, t, J =6.5 Hz, Ar-H), 7.51 (1 H, t, J = 7 Hz, Ar-H), 7.76 (1 H, d, J = 8.5 Hz, Ar-H), 7.83 (2 H, d, J = 2.0 Hz, Ar-H), 8.00 (1 H, s, Ar-H), 10.60 (1 H, s, NH), 10.64 (1 H, s, OH). **^{13}C NMR** (125 MHz, DMSO-d6), δc (ppm): 24.9 (CH_3), 106.7, 111.6 (C-Br), 118.3, 123.6, 124.3, 128.5, 131.6, 133.4, 133.6 (C-N = N-), 137.9 (C-NH), 148.9 (C-N = N-), 162.6 (C-OH), 169.2 (C═O).

(E)-N-(2-((3-bromophenyl)diazenyl)-5-hydroxyphenyl)acetamide (8). ***m*-Bromoaniline** (0.344 g, 2 mmol). **Yield** (0.214 g, 32%) as yellow solid. **m.p.** 244°C - 245°C. (**Found**: C, 50.13; H, 3.87; N, 12.50. $C_{14}H_{12}BrN_3O_2$ Requires C, 50.32; H, 3.62; N, 12.57%). ***ν*max** (cm^{-1}) 3368 (NH), 3160 (OH), 1644 (C═O), 1598 (Ar-C), 1541 (N = N), 1325 (C-N). **^{1}H NMR** (500 MHz, DMSO-d6). δH

(ppm): 2.21 (3 H, s, CH_3), 6.60 (1 H, dd, J = 9 Hz, J = 2.5 Hz, Ar-H), 7.52 (1 H, t, J = 7.5 Hz, Ar-H), 7.65 (1 H, d, J = 7.0 Hz, Ar-H), 7.69 (1 H, d, J = 8.5 Hz, Ar-H), 7.89 (1 H, s, Ar-H), 7.94 (1 H, d, J = 8.0 Hz, Ar-H), 8.13 (1 H, s, Ar-H), 10.22 (1 H, s, NH). **^{13}C NMR** (125 MHz, DMSO-d6), δc (ppm): 24.5 (CH_3), 107.2, 111.6, 119.7, 122.4 (C-Br), 123.0, 123.7, 131.1, 132.6, 133.6 (C-N = N-), 139.2 (C-NH), 153.3 (C-N = N-), 162.6 (C-OH), 168.9 (C═O).

(E)-N-(2-((4-bromophenyl)diazenyl)-5-hydroxyphenyl)acetamide (9). ***p*-Bromoaniline** (0.344 g, 2 mmol). **Yield** (0.254 g, 38%) as yellow solid. **m.p.** 246˚C - 247˚C. (**Found**: C, 50.12; H, 3.81; N, 12.75. $C_{14}H_{12}BrN_3O_2$ Requires C, 50.32; H, 3.62; N, 12.57%). ***ν*max** (cm^{-1}) 3111 (OH), 1665 (C═O), 1599 (Ar-C), 1537 (N = N), 1318 (C-N). **^{1}H NMR** (500 MHz, DMSO-d6), δH (ppm): 2.20 (3 H, s, CH_3), 6.59 (1 H, dd, J = 9.5 Hz, J = 3 Hz, Ar-H), 7.67 (1 H, d, J = 9.0 Hz, Ar-H), 7.72 (2 H, d, J = 8.5 Hz, Ar-H), 7.88 (1 H, d, J = 9.0 Hz, Ar-H), 7.92 (1 H, s, Ar-H), 10.17 (1 H, s, NH), 10.47 (1 H, s, OH). **^{13}C NMR** (125 MHz, DMSO-d6), δc (ppm): 24.6 (CH_3), 107.0, 111.5, 119.8, 123.5 (C-Br), 124.4, 132.2, 133.6 (C-N = N-), 139.0 (C-NH), 151.0 (C-N = N-), 162.2 (C-OH), 168.8 (C═O).

(*E*)-*N*-(5-hydroxy-2-((2-iodophenyl)diazenyl)phenyl)acetamide (10). ***o*-Iodoaniline** (0.219 g, 2 mmol). **Yield** (0.724 g, 95%) as a reddish orange solid, **m.p.** 249^{0}C - 250^{0}C. (**Found**: C, 44.38; H, 3.32; N, 11.16. $C_{14}H_{12}IN_3O_2$ Requires C, 44.11; H, 3.17; N, 11.02%). ***ν*max** (cm^{-1}) 3362 (NH), 3110 (OH), 1666 (C═O), 1602 (Ar- C), 1540 (N = N), 1323 (C-N). **^{1}H NMR** (500 MHz, DMSO-d6), δH (ppm): 2.23 (3 H, s, CH_3), 6.66 (1 H, dd, J = 8.5 Hz, J = 2.5 Hz, Ar-H), 7.23 (1 H, t, J = 7.5 Hz, Ar-H), 7.51 (1 H, t, J = 7.5 Hz, Ar-H), 7.77 (1 H, m, Ar-H), 7.96 (1 H, d, J = 3 Hz, Ar-H), 8.06 (1 H, d, J = 8 Hz, Ar-H), 10.35 (1 H, s, NH),10.58 (1 H. s, OH). **^{13}C NMR** (125 MHz, DMSO-d6), δc (ppm): 25.0 (CH_3), 101.5 (C-I), 107.0, 111.7, 118.0, 122.4, 129.2, 131.8, 133.6 (C-N = N-), 138.4 (C-NH), 139.4, 151.1 (C-OH), 162.5 (C-N = N-), 169.1 (C═O).

(E)-N-(5-hydroxy-2-((3-iodophenyl)diazenyl)phenyl)acetamide (11). ***m*-Iodoaniline** (0.219 g, 2 mmol). **Yield** (0.709 g, 93%) as a yellow solid, **m.p.** 252^{0}C - 253^{0}C. (**Found**: C, 44.05; H, 3.14; N, 11.32. $C_{14}H_{12}IN_3O_2$ Requires C, 44.11; H, 3.17; N, 11.02%). ***ν*max** (cm^{-1}) 3370 (NH), 3156 (OH), 1643 (C═O), 1599 (Ar-C), 1543 (N = N), 1326 (C-N). **^{1}H NMR** (500 MHz, DMSO-d6), δH (ppm): 2.20 (3 H, s, CH_3), 6.62 (1 H, d, J = 9 Hz, Ar-H), 7.37 (1 H, t, J = 8 Hz, Ar-H), 7.65 (1 H, d, J = 8.5 Hz, Ar-H), 7.83 (1 H, d, J = 7.5 Hz, Ar-H), 7.89 (1 H, s, Ar-H), 7.93 (1 H, d, J = 7 Hz, Ar-H), 8.23 (1 H, s, Ar-H), 10.19 (1 H, s, NH), 10.35 (1 H, s, OH). **^{13}C NMR** (125 MHz, DMSO-d6), δc (ppm): 24.3 (CH_3), 94.8 (C-I), 107.0, 111.3, 120.3, 122.6, 129.7, 130.9, 133.6 (C-N = N-), 138.3 (C-NH), 138.6, 153.0 (C-N = N-), 162.1 (C-OH), 168.6 (C═O).

(*E*)-*N*-(5-hydroxy-2-((4-iodophenyl)diazenyl)phenyl)acetamide (12). ***p*-Iodoaniline** (0.219 g, 2 mmol). **Yield** (0.694 g, 91%) as a yellow solid, **m.p.** 233^{0}C - 234^{0}C. (**Found**: C, 43.93; H, 3.14; N, 11.02. $C_{14}H_{12}IN_3O_2$ Requires C, 44.11; H, 3.17; N, 11.02%). ***ν*max** (cm^{-1}) 3372 (NH), 3099 (OH), 1655 (C═O), 1601 (Ar-C), 1539 (N = N), 1315 (C-N). **^{1}H NMR** (500 MHz, DMSO-d6), δH (ppm): 2.19 (3 H, s, CH_3), 6.59 (1 H, dd, J = 8.5 Hz, J = 2.5 Hz, Ar-H), 7.68 (1 H, d, J = 8.5 Hz, Ar-H), 7.70 (2 H, d, J = 8.5 Hz, Ar-H), 7.89 (1 H, d, J = 5 Hz, Ar-H), 7.92 (2 H, d, J = 2.5 Hz, Ar-H), 10.16 (1 H, s, NH), 10.49 (1 H. s, OH). **^{13}C NMR** (125 MHz, DMSO-d6), δc (ppm): 24.6 (CH_3), 97.3 (C-I), 107.1, 111.6, 119.7, 124.5, 133.7 (C-N = N-), 138.1, 139.0 (C-NH), 151.5 (C-N = N-), 162.2 (C-OH), 168.9 (C═O).

(E)-*N*-(5-hydroxy-2-(*o*-tolyldiazenyl)phenyl)acetamide (13). ***o*-Toluidine** (0.107 g, 2 mmol). **Yield** (0.366 g, 68%) as yellow solid, **m.p.** 223˚C - 224^{0}C. (**Found**: C, 66.89; H, 5.74; N, 15.33. $C_{15}H_{15}N_3O_2$ Requires C, 66.90; H, 5.61; N, 15.60%). ***ν*max** (cm^{-1}) 3365 (NH), 3096 (OH), 2919 (CH), 1658 (C═O), 1600 (Ar-C), 1538 (N = N), 1314 (C-N). **^{1}H NMR** (500 MHz, DMSO-d_6), δH (ppm): 2.20 (3 H, s, CH_3), 2.41 (3 H, s, CH_3), 6.61 (1 H, dd, J = 9.5 Hz, J = 3 Hz, Ar-H), 7.31 (1 H, d, J = 8 Hz, Ar-H), 7.43 (1 H, t, J = 6.0 Hz, Ar-H), 7.66 (1 H, d, J = 9.0 Hz, Ar-H), 7.72 (1 H, d, J = 8.0 Hz, Ar-H), 7.90 (1 H, s, Ar-H), 10.24 (1 H, s, NH), 10.45 (1 H, s, OH). **^{13}C NMR** (125 MHz, DMSO-d_6), δc (ppm): 20.9 (CH_3), 24.6 (CH_3), 107.1, 111.4, 119.6, 120.1, 123.2, 129.0, 131.1, 133.6, 138.5 (C-N = N-), 138.7 (C-NH), 152.2 (C-N = N-), 161.8 (C-O), 168.9 (C═O).

(E)-*N*-(5-hydroxy-2-(*m*-tolydiazenyl)phenyl)acetamide (14). ***m*-Toluidine** (0.107 g, 2 mmol). **Yield** (0.382 g, 71%) as yellow solid, **m.p.** 230˚C - 231˚C. (**Found**: C, 67.29; H, 5.53; N, 15.35. $C_{15}H_{15}N_3O_2$ Requires C, 66.90; H, 5.61; N, 15.60%). ***ν*max** (cm^{-1}) 3366 (NH), 3102 (OH), 2918 (CH), 1661 (C═O),1600 (Ar-C), 1539 (N = N), 1314 (C-N). **^{1}H NMR** (500 MHz, DMSO-d_6), δH (ppm): 2.20 (3 H, s, CH_3), 2.38 (3 H, s, CH_3), 6.60 (1 H, dd, J = 9 Hz, J = 2.5 Hz, Ar-H), 7.36 (1 H, d, J = 7.5 Hz, Ar-H), 7.67 (1 H, d, J = 7.5 Hz, Ar-H), 7.84 (2 H, d, J = 9.0 Hz, Ar-H), 7.91 (1 H, s, Ar-H), 10.19 (1 H, s, NH), 10.37 (1 H, s, OH). **^{13}C NMR** (125 MHz, DMSO-d_6), δc (ppm): 21.0 (CH_3), 24.6 (CH_3), 107.0, 111.3, 119.7, 122.6, 129.7, 133.5 (C-N = N-), 138.4 (C-NH-), 140.5, 150.2 (C-N = N-), 161.5 (C-O), 168.9 (C═O).

(E)-*N*-(5-hydroxy-2-(*p*-tolydiazenyl)phenyl)acetamide (15). ***p*-Toluidine** (0.107 g, 2 mmol), **Yield** (0.248 g, 46%) as yellow solid, **m.p.** 235˚C - 236˚C. (**Found**: C, 66.87; H, 5.88; N, 15.46. $C_{15}H_{15}N_3O_2$ Requires C, 66.90; H, 5.61; N, 15.60%). ***ν*max** (cm^{-1}) 3365 (NH), 3097 (OH), 2910 (CH_3), 1658 (C═O), 1601 (Ar-C), 1539 (N = N), 1314 (C-N). **^{1}H NMR** (500 MHz, DMSO-d6), δH (ppm): 2.20 (3 H, s, CH_3), 2.41 (3 H, s, CH_3), 6.59 (1 H, dd, J = 9 Hz, J = 2.5 Hz, Ar-H), 7.36 (2 H, d, J = 9 Hz, Ar-H), 7.67 (1 H, d, J = 8.5 Hz, Ar-H), 7.83 (2 H, d, J = 8 Hz, Ar-H), 7.91 (1 H, s, Ar-H), 10.19 (1 H, s, NH), 10.37 (1 H, s, OH). **^{13}C NMR** (125 MHz, DMSO-d6), δc (ppm): 21.5 (CH_3), 25.1 (CH_3), 107.5, 111.8, 120.2, 123.1, 130.2, 134.0 (C-N = N-), 138.9 (C-NH-), 141.0 (C-CH_3-), 150.7 (C-N = N-), 162.0 (C-O), 169.4 (C═O).

(*E*)-*N*-(5-hydroxy-2-((2-methoxyphenyl)diazenyl)phenyl)acetamide (16). ***o*-Anisidine** (0.246 mL, 2 mmol). **Yield** (0.394 g, 69%) as yellow, **m.p.** 227˚C - 228˚C. (**Found**: C, 62.94; H, 5.36; N, 15.01. $C_{15}H_{15}N_3O_3$ Requires C, 63.15; H, 5.30; N, 14.73%). ***ν*max** (cm^{-1}) 3426 (NH), 3116 (OH), 2929 (OCH_3), 1647 (C═O), 1596 (Ar-C), 1543 (N = N). **^{1}H NMR** (500 MHz, DMSO-d6), δH (ppm): 2.19 (3 H, s, CH_3), 3.94 (3 H, s, OCH_3), 6.66 (1 H, dd, J = 9 Hz, J = 2 Hz, Ar-H), 7.06 (1 H, t, J = 8.5 Hz, Ar-H), 7.26 (1 H, d, J = 7.5 Hz, Ar-H), 7.46 (1 H, t, J = 8.5 Hz, Ar-H), 7.71 (2 H, d, J = 9 Hz, Ar-H), 7.74 (1 H, d, J = 9 Hz, Ar-H), 8.07 (1 H, d, J = 2.5 Hz, Ar-H), 10.49 (1 H, s, NH), 11.63 (1 H, s, OH). **^{13}C NMR** (125 MHz, DMSO-d6), δc (ppm): 24.9 (CH_3), 55.8 (OCH_3), 106.1, 111.0, 113.1, 115.6, 120.7, 129.2, 132.1, 133.1 (C-N = N-), 135.7 (C-N = N-), 140.3 (C-NH), 156.0 (C-O), 161.3 (C-OH), 169.4 (C═O).

(*E*)-*N*-(5-hydroxy-2-((3-methoxyphenyl)diazenyl)phenyl)acetamide (17). ***m*-Anisidine** (0.246 mL, 2 mmol). **Yield** (0.377 g, 66%) as red, **m.p.** 200˚C - 201˚C. (**Found**: C, 63.24; H, 5.39; N, 14.59. $C_{15}H_{15}N_3O_3$ Requires C, 63.15; H, 5.30; N, 14.73%). ***ν*max**

(cm^{-1}) 3363 (NH), 3126 (OH), 2913 (OCH_3), 1650 (C═O), 1606 (Ar-C), 1543 (N = N), 1321 (C-N). **^{1}H NMR** (500 MHz, DMSO-d6), δH (ppm): 2.19 (3 H, s, CH_3), 3.84 (3 H, s, OCH_3), 6.63 (1 H, dd, J = 11.5 Hz, J = 3 Hz, Ar-H), 7.06 (1 H, dd, J = 10 Hz, J = 3 Hz, Ar-H), 7.44 (1 H, t, J = 7.5 Hz, Ar-H), 7.48 (1 H, s, Ar-H), 7.52 (1 H, d, J = 8 Hz, Ar-H), 7.68 (1 H, d, J = 8.5 Hz, Ar-H), 7.87 (1 H, d, J = 2 Hz, Ar-H), 10.21 (1 H, s, NH). **^{13}C NMR** (125 MHz, DMSO-d6), δc (ppm): 24.6 (CH_3), 55.3 (OCH_3), 106.1, 107.3, 111.6, 116.5, 116.6, 119.5, 130.0, 133.7 (C-N = N-), 138.9 (C-N = N-), 153.5 (C-NH), 160.0 (C-O), 162.0 (C-OH), 168.9 (C═O).

(*E*)-*N*-(5-hydroxy-2-((4-methoxyphenyl)diazenyl)phenyl)acetamide (18). ***p*-Anisidine** (0.246 g, 2 mmol). **Yield** (0.399 g, 70%) as yellow, **m.p.** 234°C - 235°C. (**Found**: C, 63.08; H, 5.37; N, 14.38. $C_{15}H_{15}N_3O_3$ Requires C, 63.15; H, 5.30; N, 14.73%). ***ν*max** (cm^{-1}) 3660 (NH), 3103 (OH), 2999 (OCH_3), 1663 (C═O), 1603 (Ar-C), 1549 (N = N). **^{1}H NMR** (500 MHz, DMSO-d6), δH (ppm): 2.20 (3 H, s, CH_3), 3.84 (3 H, s, OCH_3), 6.59 (1 H, dd, J = 9 Hz, J = 3 Hz, Ar-H), 7.09 (2 H, d, J = 9.0 Hz, Ar-H), 7.65 (1 H, d, J = 8.5 Hz, Ar-H), 7.93 (3 H, d, J = 9.5 Hz, Ar-H), 10.15 (1 H, s, NH). **^{13}C NMR** (125 MHz, DMSO-d6), δc (ppm): 24.6 (CH_3), 55.5 (OCH_3), 107.0, 111.3, 114.4, 119.4, 124.4, 133.5 (C-N = N-), 138.2 (C-N = N-), 146.4 (C-NH), 161.1 (C-O), 161.2 (C-OH), 168.8 (C═O).

2.3. Antibacterial evaluation

2.3.1. Kirby-Bauer disc diffusion method

The initial antibacterial activity of the compounds **1–18** was screened by adapting the Kirby-Bauer disc diffusion method from Desai *et al.* (2022) [25]. Approximately 20 mL of sterile Mueller-Hinton Agar was poured into each of the petri dishes and allowed to cool to room temperature for solidification under aseptic conditions. Two bacterial strains with Gram-positive (*Staphylococcus aureus*) and Gram-negative (*Escherichia coli*) were chosen for the antibacterial evaluation [26] owing to their pathogenic nature and frequent occurrences in healthcare settings [27]. The bacteria were adjusted to a 0.5 McFarland standard, which is equivalent to 1.5×10^8 CFU/mL of cell density [28]. The 100 µL of bacterial suspensions were uniformly swabbed onto the petri dishes with Mueller-Hinton Agar using a sterile cotton swab and left dry for 15 min by following the standard guidelines from Clinical and Laboratory Standard Institute (CLSI) [29]. The 10 µL compounds were prepared by dissolving 10 mg of compound in 1 mL DMSO, giving the final DMSO concentration of approximately 1% (v/v), which is below the threshold known to cause inhibitory effects on bacterial growth. The sterile discs (6 mm diameter) were impregnated with 10 µL of the synthesised compounds **1–18** and gently pressed on the agar surface. Ampicillin and DMSO were used as positive and negative controls, respectively. The plates were then incubated at 37°C for 24 h before measuring the inhibition zone of the discs in millimetres (mm).

2.3.2. Turbidimetric kinetic method

Compounds **1 (*o*-F)**, **2 (*m*-F)**, **5 (*m*-Cl)** and **14 (*m*-CH_3)** with prominent activities in the initial disc diffusion screening were further subjected to minimum inhibitory concentration (MIC) determination using the Turbidimetric Kinetic Method [30]. The Luria-Bertani broth was used to culture the bacteria under optimum conditions in an incubator shaker (120 rpm) for 24 h. Compounds at different concentrations of 50 ppm, 80 ppm and 100 ppm were added to respective bottles containing 10 mL of Luria-Bertani broth and inoculated with 200 µL of inoculum. The mixture was shaken for 6 h in an incubator shaker at 120 rpm. For every interval of 1 h, 1000 µL of aliquots in different concentrations was pipetted out into a cuvette to measure the transmittance value. The reading was obtained by using a UV-visible spectrophotometer at a 560 nm wavelength. Each concentration of the compounds was done in triplicate to obtain the mean reading of the transmittance value (Supplementary data S57-S98). The standard deviation of the replicates was calculated, and the Relative Standard Deviation (RSD) is within an acceptable range for a biological assay of less than 20% [31]. The data were presented as mean ± SD, and one-way analysis of variance (ANOVA) statistical treatment was performed with all datasets achieving $p < 0.05$. Then, the transmittance values obtained were used to determine the number of colony-forming units (CFU) mL^{-1} formed against time by substituting the value into Eqs. (1) and (2) according to the bacteria strain. Subsequently, the values obtained were subjected to Eq. (3) in order to derive the specific growth rate of the bacteria when $\mu = 0$. The minimum inhibition concentration (MIC) was determined by extrapolating the graph of specific growth rate versus concentration.

$$S.\ aureus: \ln N_t = 27.4 - 10.3\,T \quad (1)$$

$$E.\ coli: \ln N_t = 27.1 - 8.56\,T \quad (2)$$

$$\mu = (\ln N_t - \ln N_0)/(t - t_0) \quad (3)$$

2.4. Molecular Docking

The 2D structure of selected synthesised compounds was drawn using Discovery Studio® 4.0 (Accelrys, San Diego, USA) and saved in PDB format, followed by geometry and energy optimisation using Avogadro [32], employing the steepest descent and conjugated gradient method, using the MMFF94 force field. The crystal structure of the FtsA enzyme (PDB ID: 3WQU) was downloaded from the Protein Data Bank (PDB). Hydrogen atoms were added to the FtsA enzyme structure using AutoDockTools [33] while the docking was performed using AutoDock Vina, with a grid box for FtsA enzyme set 40 × 30 x 40 and 1.0 Å spacing [34]. The grid box was set to be 1.0 Å so that all the residues were available in an equal-opportunity zone for ligand binding. The docked ligand binding was ranked according to its binding energies. The highest binding affinity was selected, and the binding interactions were visualised using Discovery Studio® 4.0 (Accelrys, San Diego, USA). This ligand conformation was carefully inspected, analysed, and discussed. To verify the docking parameters, redocking of the Adenosine-5′-Triphosphate, which is present in the FtsA enzyme crystal protein

structure, was done. The redocking for Adenosine-5′-Triphosphate was performed using AutoDock Vina with the parameters described above.

2.5. ADME prediction

The online software SwissADME tool (http://www.swissadme.ch/index.php) was carried out by inserting the SMILE notation of the compounds [35,36]. The computational studies have become indispensable as they have acted as a guidance for drug discovery in the initial stages and improved previous statistics of 50% of drug candidates being rejected in the development stage [37]. This would be an advantage for researchers as it has improved accuracy, reduced the time and cost of drug development [38,39]. The integration of computer technology ADME would improve understanding of compound behaviours from aspects such as pharmacokinetics, physicochemical, toxicity, lipophilicity, water solubility and drug-likeness characteristics [40,41]. The following formula was used to determine the oral absorption rate (%): ABS = 109 – [0.345 ⨷ Topological polar surface area(TPSA)] [42].

3. results and discussion

3.1. Synthesis and structural characterisation

The synthesis of metacetamol azo derivatives **1–18,** as shown in Fig. 1, was achieved *via* two classical steps of reaction that involve diazotisation and coupling reaction with electron-rich aromatic compounds [43]. The substituted anilines were reacted with sodium nitrite under low temperature (0–5℃) in acidic conditions to form diazonium salt. The reaction was maintained at a low temperature to ensure stability of the diazonium salt [44]. The mixture was monitored closely by using potassium iodide-starch paper, whereby transformation to a purple-blue colour indicates formation of nitrous acid [45], signifying the progress of the diazotisation reaction. Subsequently, the metacetamol in alkaline conditions serves as an electron-rich aromatic coupling reagent, which was added into the diazonium salt solution to yield the targeted metacetamol azo **1–18** in low to high yield of 32–95%.

The structure of metacetamol azo **1–18** was elucidated by using FTIR and NMR spectroscopies (Supplementary data, Figures S1-S54). The significant FTIR absorption band detected around 1550 cm^{-1} was attributed to the formation of an azo bond [46]. The peaks at 3368–3458 cm^{-1} and 3089–3160 cm^{-1} corresponded to the presence of amide ν(NH) and hydroxyl ν(OH) from the metacetamol core structure, respectively [47,48]. The assignment of ν(NH) at a higher wavenumber was due to the structural composition and position of the heteroatom derivatives, which demonstrated a more stable hydrogen bond than ν(OH) [49]. Moreover, the ν(OH) band typically appears broad due to intermolecular hydrogen bonding, while the ν(NH) vibration is relatively narrower and features a pointy peak [50]. Whereas the strong absorption band at lower frequencies of 1643–1646 cm^{-1} were assigned to the stretching vibrations of the carbonyl functional group, ν(C═O) [51].

The compounds were further confirmed by characterising using ^{1}H and ^{13}C NMR analysis. Chemical shift in NMR is one of the most reliable techniques to be used for molecular assignment and structure elucidation due to the high sensitivity of chemical environment towards the surrounding nucleus [52]. In ^{1}H NMR spectra, the most upfield singlet proton found at 2.15 ppm – 2.22 ppm was attributed to the CH_3 proton due to the high shielding effect [53] and the electron-donating nature of the methyl group that forms a CH···π interaction [54]. In contrast, two singlet peaks were observed at the most downfield region of 10.35 – 11.63 ppm and 10.12 ppm – 10.73 ppm were assigned to the hydroxyl group (OH) and amide group (NH), respectively. This is due to the high polarizability of the surrounding electronic environment of groups with oxygen and nitrogen atoms that reduces electron density, resulting in a high deshielding effect, hence shifting the proton towards a more downfield region [55]. However, the hydroxyl peak for compounds **1 (*o*-F)**, **2 (*m*-F)**, **3 (*p*-F)**, **4 (*o*-Cl)**, **8 (*m*-Br)**, **17 (*o*-CH_3)** and **18 (*p*-OCH_3)** was not observed due to its labile property [56]. In ^{13}C NMR, peaks resonating at 24.3–25.0 ppm were attributed to the CH_3 peak. Meanwhile, the carbonyl group (C═O) resonate at the most downfield region of 169.3 ppm – 169.3 ppm due to the high electronegativity of the oxygen atom [57,58]. Additionally, peaks at 106.5 ppm to 138.6 correspond to aromatic carbon, whereas C-N = N- of the azo linker found at 133.1–162.5 ppm [59].

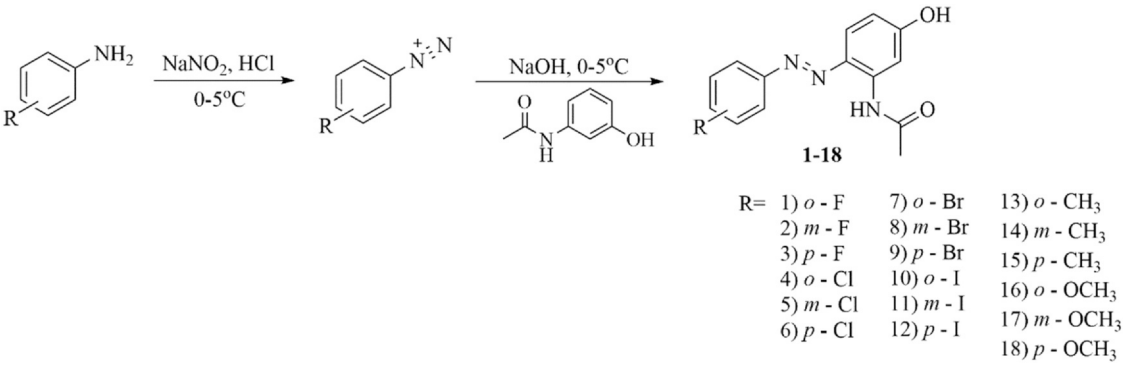

Fig. 1. Synthesis of metacetamol azo derivatives **(1 – 18)**.

3.2. Antibacterial evaluation

In this study, the initial *in vitro* antibacterial screening of metacetamol azo **1–18** was evaluated towards Gram-positive bacteria (*Staphylococcus aureus*) and Gram-negative bacteria (*Escherichia coli*) using the Kirby-Bauer disc diffusion method. This screening is to provide a qualitative indication of activity to identify candidates for further analysis. The two bacteria were deployed due to their ability to mutate swiftly to develop as multidrug-resistant bacteria and their fast-growing ability [60]. Moreover, both strains have been seen as causes of superficial and systemic infections [61], which estimated that antimicrobial-resistant bacteria would cause a hundred million deaths worldwide in 2050 [62]. With ampicillin as the standard drug and DMSO as a negative control, the zone of inhibition of each compound was measured, and the results were tabulated as in Table 1.

Overall, the newly synthesised compounds (*except compound **16***) have shown promising antibacterial potential compared to metacetamol, with no inhibition likely reflecting the presence of azo bonds that enhance binding affinity towards the enzyme's active site of the microbes, potentially *via* formation of hydrogen bonding [63]. Moreover, an additional phenyl ring from the aniline derivative boosts the interaction with proteins of bacteria *via* numerous intermolecular forces such as π-π stacking effects [64], hydrogen bonding, hydrophobic interaction, dipole-induced dipole and *van der Waals* forces [65] that would disrupt the cytoplasmic membrane [66].

Notably, fluorine-substituted compounds **2 (*m*-F)** have shown the most potent activity towards *E. coli* strains with an inhibition zone of 12 mm, owing to the ideal positioning and small atomic size of the fluorine atom that would cause less steric hindrance between the active site of the bacterial membrane and compounds that contribute to effective membrane disruption [30]. The C-F bond of fluorinated compounds has a high dissociation energy of 105.4 kcal/mol, making it less likely to undergo metabolic and enzymatic transformation [67,68], allowing the compounds to have a longer duration of reaction and better bioavailability [69]. Comparatively, the least active of *para*-fluorine substituted may be due to the compensation of both resonance and inductive effect, resulting in a less acidic compound [70]. Other halogenated substituted compound series (**1–12)** also show promising inhibitions against both strains, comparable to standard ampicillin, probably due to the increase in lipophilicity attributed to the inductive effect [71] and electro-negative nature of the substituent, which improves the interaction between the enzyme-active sites and receptor-recognition sites of the compounds [72].

Upon comparing the electron-donating substituted series (**13–18**), the presence of a moderate electron-donating group, methyl, exhibited better inhibition ability than a strong electron-donating group of the methoxy [73], especially towards *E. coli*. This may be due to methyl's favourable balance of electron donation (inductive donating) without the strong resonance delocalisation associated with methoxy, thereby preserving molecular lipophilicity and enhancing cell membrane penetration and binding to bacterial targets [74].

The finding also indicates metacetamol-azo **1–18** is relatively less susceptible to Gram-negative bacteria (*E. coli*) as compared to Gram-positive bacteria (*S. aureus*). This may be due to the permeability barriers of Gram-negative bacteria that are densely packed with lipopolysaccharides on the outer leaflet [75,76] and an asymmetric phospholipid bilayer on the inner leaflet [77]. In contrast, Gram-positive bacteria lack an outer membrane, consisting only of a thick peptidoglycan layer, which is more sensitive [78,79] and is easily penetrated by antibacterial drugs [80].

The selected compounds **1 (*o*-F)**, **2 (*m*-F)**, **5 (*m*-Cl)** and **14 (*m*-CH_3)** with prominent activities in preliminary screening were further examined with the turbidimetric kinetic method to determine their minimum inhibitory concentration (MIC). The MIC is the smallest concentration of an antimicrobial agent that prevents visible growth after overnight incubation, and it is used to verify the resistance of microorganisms to the antibacterial agent. At the concentrations of 50 ppm, 80 ppm, and 100 ppm against *S. aureus* and *E. coli,* the transmittance values obtained were subjected to the equation of colony-forming units $(CFU)mL^{-1}$ ($\ln Nt$) versus time of each strain. Extrapolating the concentration at the specific growth rate of bacteria, following the expression of Eq. 3, gave the MIC values as tabulated in Table 2**,** and the graph is in Supplementary **S55-S56.** The MIC values were categorised as significant if below 100 ppm, moderate when $100 \leq MIC \leq 625$ ppm and weak when $MIC > 625$ ppm [81]. Compounds exhibiting MIC values below 200 ppm are considered promising antimicrobial candidates and can be suggested for pharmacological purposes [82].

Table 1
Zone of inhibition of compound **1–18.**

Compound	Diameter of inhibition zone (mm)		Compound	Diameter of inhibition zone (mm)	
	S. aureus	*E. coli*		*S. aureus*	*E. coli*
1 (*o*-F)	8	7	**12 (*p*-I)**	-	7
2 (*m*-F)	7	12	**13 (*o*-CH_3)**	9	-
3 (*p*-F)	8	-	**14 (*m*-CH_3)**	8	7
4 (*o*-Cl)	8	-	**15 (*p*-CH_3)**	9	-
5 (*m*-Cl)	8	7	**16 (*o*-OCH_3)**	-	-
6 (*p*-Cl)	8	-	**17 (*m*-OCH_3)**	7	-
7 (*o*-Br)	7	-	**18 (*p*-OCH_3)**	8	-
8 (*m*-Br)	-	7	**Metacetamol**	-	-
9 (*p*-Br)	7	-	**Ampicillin**	7	7
10 (*o*-I)	7	-	**DMSO**	-	-
11 (*m*-I)	7	-			

Note: (-) = no activity; *o* = ortho, *m* = meta, *p* = para

Table 2
Minimum inhibitory concentration of selected compounds.

Compound	Minimum inhibitory concentration (ppm)		Compound	Minimum inhibitory concentration (ppm)	
	E. coli	*S. aureus*		*E. coli*	*S. aureus*
1 (*o*-F)	155.25	142.65	**14 (*m*-CH_3)**	200.11	151.82
2 (*m*-F)	147.47	108.67	**Ampicillin**	118.14	98.79
5 (*m*-Cl)	172.67	176.51	**DMSO**	-	-

Note: (-) = no activity; *o* = ortho, *m* = meta, *p* = para

The MIC data showed a similar inhibition trend as in the disc diffusion screening test. Upon comparing fluoro-substituted compound **1 (*o*-F)** and **2 (*m*-F)**, the latter exhibited stronger bacteriostatic activity. This *meta*-effect portrayed by **2 (*m*-F)** is attributed to the dominance of the inductive effect (-I) at the meta-position, which enhances the lipophilicity and membrane-binding affinity of the compound [71,91]. Unlike *para*-substitution, where the resonance effect (+R) can partially counteract the inductive electron withdrawal, potentially reducing the acidity and binding affinity of the molecule [70]. In contrast, the lower activity of the *ortho* derivative, **1 (*o*-F)**, likely stems from localised steric crowding near the pharmacophore, which may distort the optimal binding conformation, reducing the antibacterial activity [83]. Furthermore, the fluorine-substituted compounds depicted higher activity than chlorine, **5 (*m*-Cl).** This is exerted by the ability of fluorine to withdraw a larger amount of electron density, leading to higher cationic property and acidity, resulting in better electrostatic interaction with the negatively charged bacterial cell membrane, altering the lipid bilayer structure of the cell [84]. Conversely, compound **14 (*m*-CH_3)** with an electron-donating group showed reduced antibacterial activity due to higher electron density [73] that alters the electronic distribution and hinders membrane penetration ability [22].

3.3. Molecular docking

In this study, the FtsA enzyme was chosen as the therapeutic target because it plays a crucial role in bacterial cell division and replication in many bacterial species [85]. FtsA belongs to the actin/MreB family of proteins and possesses ATP-binding sites [86]. By targeting the ATP-binding site in FtsA, the cell division and replication will be inhibited, subsequently causing cell death. In the docking procedure, the redocking step with Adenosine-5′-Triphosphate, the FtsA enzyme co-crystal was performed to verify the

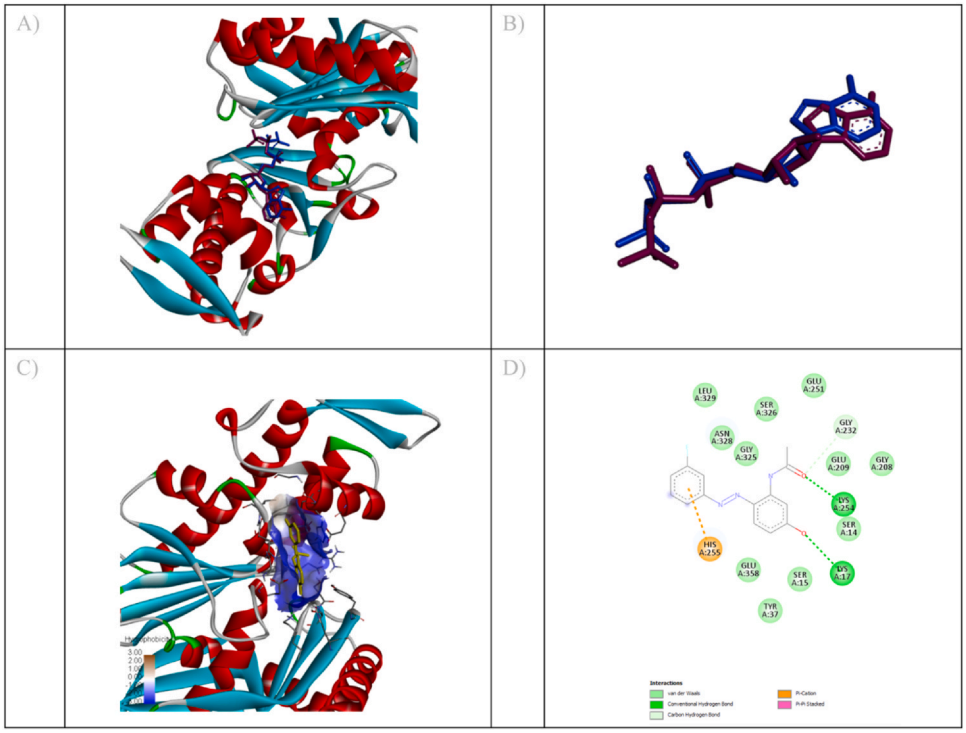

Fig. 2. Diagrams showing (A) the alignment of the redocked Adenosine-5′-Triphosphate (purple stick model) and Adenosine-5′-Triphosphate co-crystallized (blue stick model) within the binding site of FtsA; (B) superimposition of redocking Adenosine-5′-Triphosphate (purple stick model) and Adenosine-5′-Triphosphate crystal (blue stick model); (C) compound **2 (*m*-F)** within the binding site of FtsA; (D) the 2D schematic diagram of residues in the binding site of FtsA exhibiting hydrogen bond (green dotted line) and μ-cation interaction (orange dotted line) with compound **2 (*m*-F)** visualized and analyzed by using Discovery Studio 4.0.

docking parameter used in this study [87]. This was done to ensure the reproducibility of the docking outputs. The orientation of the best docking pose of Adenosine-5′-Triphosphate was superimposed with the original crystal structure of Adenosine-5′-Triphosphate at the ATP binding site of the crystal structure. The root mean square derivative (RMSD) value between the top-ranked docked Adenosine-5′-Triphosphate conformation and the co-crystal pose of Adenosine-5′-Triphosphate was found to be 1.6171 Å **(**Fig. 1**)**. It was observed that both docked conformations of the inhibitor had a similar orientation with a crystallised inhibitor in the crystal structure from the redocking study, suggesting that AutoDock Vina has high accuracy in terms of predicting the binding interactions of the ligand of interest with the crystal structure [88].

Thereafter, the docking was performed on the selected metacetamol azo compounds **1 (*o*-F)**, **2 (*m*-F), 5 (*m*-C1)** and **14 (*m*-CH_3),** which showed promising antibacterial activity toward both bacterial strains tested in the *in vitro* studies earlier. This is to investigate the mechanism of action of how these compounds particularly cause inhibition at the molecular level. As illustrated in Fig. 1**,** visualised by Discovery Studio 4.0, the major similarities of these selected compounds are that there are multiple hydrogen bonding interactions present to the amino acid of the FtsA enzyme, leading to high binding energy ranging from −8.2 to −9.4 kcal/mol. Meanwhile, the positive control, ampicillin, possessed a binding energy of −9.0 kcal/mol. For compound **2 (*m*-F),** with the highest inhibition towards *E. coli*, the establishment of two hydrogen bonds with the important amino acids, LYS 17 and LYS 254, is similar to those observed in ampicillin and Adenosine-5′-Triphosphate co-crystal, respectively. These two amino acids, located at the active site of the FtsA enzyme, are important for cell structural integrity through FtsA-FtsA interaction and/or with other essential division components like FtsZ, at which disruption by an inhibitor allosterically inhibits FtsA function [89,90]. This is likely driven by the strategic *meta*-substitution of the fluorine atom, which acts as a powerful electron-withdrawing group. By inductively polarising the molecular scaffold, the fluorine enhances the electrostatic complementarity of neighbouring atoms, thereby optimising the strength of the hydrogen bonds with the key residues [67,91]. Additionally, *van der Waals* interaction with GLU 251 and μ-cation interaction with HIS255 were also found. Moreover, several key residues were also observed in the vicinity (GLY 325, SER 14, GLU 209). Disturbances to these amino acids will lead to ribose destabilisation, thus stopping the bacteria's replication or cell division [92]. The detailed binding illustration can be retrieved from Supplementary data, **S99**, while the binding summary of the selected compound is tabulated in Table 3.

3.4. ADME prediction

Physicochemical, pharmacokinetic and toxicity properties of metacetamol-azo **1–18** are studied *via* SwissADME to examine the absorption, distribution, metabolism and excretion (ADME) properties and predict its druglikeness properties. The SwissADME is a fast and yet free online access tool that would be able to provide modest predictive results [93,94]. The physicochemical properties of the compounds were tabulated in Table 4. None of the compounds violated the Pfizer Rule, also known as Lipinski's rule of five, with molecular weight (MW) ⩽ 500 g/mol, number of hydrogen bond donors (nHBD) ⩽ 5, number of hydrogen bond acceptors (nHBA) ⩽ 10, Topological polar surface area (TPSA) ⩽ 140Å^2 and Log P value ⩽ 5.0 [95]. Compounds without breaking more than one of Lipinski's rules are expected to display good intestinal permeability and aqueous solubility [37]. Based on the result, metacetamol-azo **1–18** were detected to have ⩾ 3 rotatable bonds, indicating good molecular flexibility [96] and high oral bioavailability with all the topological polar surface area (TPSA) values less than 140Å^2 [97,98]. The absorption value of the compounds, ranging from 80.27% to 83.45%, was derived by using the formula [109 – (0.345 ⨩ TPSA)] [99]. This is aligned with the predicted solubility, which belongs to the range of moderately soluble to soluble.

The druglikeness of metacetamol-azo **1–18** was organised in Table 5 according to the different pharmacokinetic rules reported. Interestingly, all compounds **1–18** abide by all criteria of the rules tested below except for metacematol, which violated the Ghose filter and Muegge rules due to low molecular weight.

- Ghose filter: (160 ⩽ MW ⩽ 480, 20 ⩽ Number of atoms ⩽ 70, 40 ⩽ MR ⩽ 130 & −0.4 ⩽ Log P ⩽ 5.6). Emphasising the compound's lipophilicity and molar refractivity, significant for receptor binding, cellular absorption and bioavailability [100].
- Veber: (TPSA ⩽ 131.6 Å^2 & nRotB ⩽ 10). Prioritise on surface area and flexibility of the molecule, criteria that influence the oral bioavailability and permeability [101,102].
- Egan: (TPSA ⩽ 131.6 Å^2 & Log P > 5.88). Explains the balance of hydrophilic and hydrophobic properties of compounds [101,103].
- Muegee: (200 ⩽ MW ⩽ 600, nHBD ⩽ 5, nHBA ⩽ 10, nrotb ⩽ 15, TPSA ⩽ 150 Å^2, −2 ⩽ Log P ⩽ 5, number of rings ⩽ 7, number of heteroatoms > 1 & number of carbons > 4). An additional condition ensuring the drugs follow the druglikeness properties) [101,104].

Table 3
Molecular docking interaction of selected compounds towards FtsA enzyme (PDB ID: 3WQU).

Compounds	Binding affinity (kcal/mol)	Key Binding residues
1 (*o*-F)	-8.8	SER15, GLY232, LEU329, HIS255, ASN328, GLU358
2 (*m*-F)	-9.4	HIS255, LYS17, LYS254, GLY232
5 (*m*-C1)	-8.6	LYS17, GLY325, SER14, HIS255, LYS254, SER15
14 (*m*-CH_3)	-8.2	GLY325, LYS77, SER361, ASP185, VAL211, GLU209, ASP210
Ampicillin	-9.0	ASN328, HIS255, GLU358, GLY325, LYS17, SER15

Table 4
Physicochemical properties of compound **1–18**.

Compound	MW[a]	nHA[b]	nAHA[c]	nRotB[d]	nHBA[e]	nHBD[f]	MR[g]	TPSA[h]	ABS[i]	MLOGP[j]	ESOL[k]
1 (*o*-F)	273.26	20	12	4	5	2	73.35	74.05	83.45	2.38	S
2 (*m*-F)	273.26	20	12	4	5	2	73.35	74.05	83.45	2.38	S
3 (*p*-F)	273.26	20	12	4	5	2	73.35	74.05	83.45	2.38	S
4 (*o*-Cl)	289.72	20	12	4	4	2	78.41	74.05	83.45	2.51	S
5 (*m*-Cl)	289.72	20	12	4	4	2	78.41	74.05	83.45	2.51	S
6 (*p*-Cl)	289.72	20	12	4	4	2	78.41	74.05	83.45	2.51	S
7 (*o*-Br)	334.17	20	12	4	4	2	81.1	74.05	83.45	2.63	MS
8 (*m*-Br)	334.17	20	12	4	4	2	81.1	74.05	83.45	2.63	MS
9 (*p*-Br)	334.17	20	12	4	4	2	81.1	74.05	83.45	2.63	MS
10 (*o*-I)	381.17	20	12	4	4	2	86.11	74.05	83.45	2.76	MS
11 (*m*-I)	381.17	20	12	4	4	2	86.11	74.05	83.45	2.76	MS
12 (*p*-I)	381.17	20	12	4	4	2	86.11	74.05	83.45	2.76	MS
13 (*o*-OCH_3)	269.3	20	12	4	4	2	78.36	74.05	83.45	2.24	S
14 (*m*-OCH_3)	269.3	20	12	4	4	2	78.36	74.05	83.45	2.24	S
15 (*p*-OCH_3)	269.3	20	12	4	4	2	78.36	74.05	83.45	2.24	S
16 (*o*-OCH_3)	285.3	21	12	5	5	2	79.89	83.28	80.27	1.7	S
17 (*m*-OCH_3)	285.3	21	12	5	5	2	79.89	83.28	80.27	1.7	S
18 (*p*-OCH_3)	285.3	21	12	5	5	2	79.89	83.28	80.27	1.7	S
Metacetamol	151.16	11	6	2	2	2	42.78	49.33	91.98	1.25	S

Note: [a]Molecular weight (MW); [b]Number of heavy atom (nHA); [c]Number of aromatic heavy atom (nAHA), [d]Number of rotatable bonds (nRotB); [e]Number of hydrogen bond acceptors (nHBA); [f]Number of hydrogen bond donors (nHBD); [g]Molecular refractivity (MR); [h]Topological polar surface area (TPSA); [i]Absorption value in percentage (ABS); [j]Octanol/water partition coefficient (MLOGP); and Estimate solubility (ESOL) with S representing soluble and MS representing moderately soluble.

Table 5
Druglikeness of compound **1–18**.

Compound	Lipinski	Ghose	Veber	Egan	Muegee	PAINS[a]	Brenk
1 (*o*-F)	Yes	Yes	Yes	Yes	Yes	1	1
2 (*m*-F)	Yes	Yes	Yes	Yes	Yes	1	1
3 (*p*-F)	Yes	Yes	Yes	Yes	Yes	1	1
4 (*o*-Cl)	Yes	Yes	Yes	Yes	Yes	1	1
5 (*m*-Cl)	Yes	Yes	Yes	Yes	Yes	1	1
6 (*p*-Cl)	Yes	Yes	Yes	Yes	Yes	1	1
7 (*o*-Br)	Yes	Yes	Yes	Yes	Yes	1	1
8 (*m*-Br)	Yes	Yes	Yes	Yes	Yes	1	1
9 (*p*-Br)	Yes	Yes	Yes	Yes	Yes	1	1
10 (*o*-I)	Yes	Yes	Yes	Yes	Yes	1	2
11 (*m*-I)	Yes	Yes	Yes	Yes	Yes	1	2
12 (*p*-I)	Yes	Yes	Yes	Yes	Yes	1	2
13 (*o*-OCH_3)	Yes	Yes	Yes	Yes	Yes	1	1
14 (*m*-OCH_3)	Yes	Yes	Yes	Yes	Yes	1	1
15 (*p*-OCH_3)	Yes	Yes	Yes	Yes	Yes	1	1
16 (*o*-OCH_3)	Yes	Yes	Yes	Yes	Yes	1	1
17 (*m*-OCH_3)	Yes	Yes	Yes	Yes	Yes	1	1
18 (*p*-OCH_3)	Yes	Yes	Yes	Yes	Yes	1	1
Metacetamol	Yes	No	Yes	Yes	No	1	0

Note: [a]Pan assay interferences structures (PAINS)

In regard to the distribution factor as tabulated in Table 6, all compounds **1–18** showed high gastrointestinal (GI) absorption. This is an advantage for drug candidates as it is readily available for efficient and convenient oral administration [105]. Most of the compounds are able to diffuse through the blood-brain barrier except for methoxy-substituted compounds **16 – 18** due to a comparatively higher TPSA value [106]. Observation of the compounds' diffusion through Cytochromes P450 (CYP) isoforms indicated active diffusion to CYP1A2, CYP2C19 (except **1–3** ***(F-substituted)*** and **16–18** ***(-OCH_3 substituted)*** and CYP2C9 (except compounds **1–3 (*F-substituted*)**. These CYP450 isoforms play an important role in metabolising or oxidising the drugs to facilitate the drug excretion from the body [107,108]. All compounds are inactive against CYP2D6 and CYP3A4. The result of metacetamol alone showed that there is no balance in inhibiting the CYP450 isoforms, which may cause accumulation toxicity if it is not excreted through an alternative pathway [109]. Finally, the compounds were predicted to have low skin permeability (log Kp) with the value ranging from −5.83 to −6.37 cm/s, indicating these compounds were not suitable for transdermal medication [110].

Table 6
Pharmacological properties of compound **1–18**.

Compound	GI[a]	BBB[b]	P-gp[c]	CYP1A2[d]	CYP2C19[e]	CYP2C9[f]	CYP2D6[g]	CYP3A4[h]	Log Kp (cm/s)
1 (*o*-F)	High	Yes	No	Yes	No	No	No	No	-6.11
2 (*m*-F)	High	Yes	No	Yes	No	No	No	No	-6.11
3 (*p*-F)	High	Yes	No	Yes	No	No	No	No	-6.11
4 (*o*-Cl)	High	Yes	No	Yes	Yes	Yes	No	No	-5.83
5 (*m*-Cl)	High	Yes	No	Yes	Yes	Yes	No	No	-5.83
6 (*p*-Cl)	High	Yes	No	Yes	Yes	Yes	No	No	-5.83
7 (*o*-Br)	High	Yes	No	Yes	Yes	Yes	No	No	-6.06
8 (*m*-Br)	High	Yes	No	Yes	Yes	Yes	No	No	-6.06
9 (*p*-Br)	High	Yes	No	Yes	Yes	Yes	No	No	-6.06
10 (*o*-I)	High	Yes	No	Yes	Yes	Yes	No	No	-6.37
11 (*m*-I)	High	Yes	No	Yes	Yes	Yes	No	No	-6.37
12 (*p*-I)	High	Yes	No	Yes	Yes	Yes	No	No	-6.37
13 (*o*-OCH_3)	High	Yes	No	Yes	Yes	Yes	No	No	-5.9
14 (*m*-OCH_3)	High	Yes	No	Yes	Yes	Yes	No	No	-5.9
15 (*p*-OCH_3)	High	Yes	No	Yes	Yes	Yes	No	No	-5.9
16 (*o*-OCH_3)	High	No	No	Yes	No	Yes	No	No	-6.27
17 (*m*-OCH_3)	High	No	No	Yes	No	Yes	No	No	-6.27
18 (*p*-OCH_3)	High	No	No	Yes	No	Yes	No	No	-6.27
Metacetamol	High	Yes	No	No	No	No	No	No	-6.27

Note: [a]Gastrointestinal absorption (GI); [b]Blood-brain barrier permeability (BBB); [c]Permeability glycoprotein substrate (P-gp), [d]CYP1A2 inhibitor (CYP1A2); [e]CYP2C19 inhibitor (CYP2C19); [f]CYP2C9 inhibitor (CYP2C9); [g]CYP2D6 inhibitor (CYP2D6) and [h]CYP3A4 inhibitor (CYP3A4)

3.5. Study limitations

While the findings of this study provide a promising foundation for the development of metacetamol-based antibacterials, several limitations must be acknowledged. To note, this study focused exclusively on two standard bacterial strains: the Gram-positive *Staphylococcus aureus* (ATCC 25923) and the Gram-negative *Escherichia coli* (ATCC 25922). Even though these are clinically significant pathogens, they do not represent the full diversity of bacterial species. Future studies should expand testing to include clinical isolates and a broader range of multidrug-resistant (MDR) strains to better determine the clinical utility of these derivatives. Furthermore, the pharmacological assessment is currently restricted to initial *in vitro* screening and *in silico* modelling. Consequently, further *in vivo* pharmacological and toxicity evaluations in animal models are essential to validate these compounds as safe and effective therapeutic candidates. Finally, the pharmacokinetic and drug-likeness assessments were conducted using the SwissADME online tool, which provides predictive trends rather than experimental data. While these computational models are indispensable for early-stage drug discovery, they do not fully account for the complex metabolic transformations that occur *in vivo*. Experimental pharmacokinetic studies are therefore necessary to confirm these predictions. Despite these constraints, the findings provide a structural foundation for the future optimisation and rigorous biological testing of the metacetamol azo scaffold.

4. Conclusion

A series of metacetamol azo derivatives **1–18** was successfully synthesised and structurally characterised *via* spectroscopic techniques. The findings demonstrated that the incorporation of the azo linker (-N = N-) combined with *o*, *m* and *p*-F/Cl/Br/ I/CH_3/ OCH_3 substituents of aniline significantly enhanced the antibacterial properties relative to the parent drug, metacetamol. Among the synthesised compounds, **2 (*m*-F)** exhibited promising antibacterial activity with MIC values of 108.67 ppm for *S. aureus* and 147.47 for *E. coli,* comparable to standard ampicillin (98.79 ppm for *S. aureus* and 118.14 ppm for *E. coli*). This enhanced activity is likely attributed to optimal electronic, positioning and steric characteristics of the fluorine substituent. Molecular docking analysis further supported the *in vitro* finding, revealing the strong binding affinity (-9.4 kcal/mol) of **2 (*m*-F)** toward key residues within the active site of the bacterial cell division of the FtsA enzyme. In addition, computational ADME studies revealed that metacetamol-azo **1–18** possessed favourable physicochemical and pharmacokinetic profiles, suggesting promising drug-like characteristics and supporting their potential as biologically active agents. Overall, the present study collectively demonstrates that strategic azo functionalisation of metacetamol provides a useful structural design for the development of new antibacterial scaffolds with enhanced antibacterial potency. Nevertheless, further detailed mechanism-of-action investigations, *in vivo* pharmacological and toxicity evaluations are necessary to further validate these compounds as potential therapeutic candidates.

CRediT authorship contribution statement

Aina Syakirah Mohammad Hussin: Methodology, Investigation, Formal analysis. **Wan Sharifatun Handayani Wan Zullkiplee:** Writing – review & editing. **Halvy Hilary David:** Methodology, Investigation, Formal analysis. **D'artaqnand Daniel:** Methodology, Investigation, Formal analysis. **Nur Izzah Haziyah Ishak:** Methodology, Investigation, Formal analysis. **Matherine Sadiah Mathew:** Methodology, Investigation, Formal analysis. **Davlye Noissy Diosing:** Methodology, Investigation, Formal

analysis. **Nur Alia Syahilda Zikri:** Methodology, Investigation, Formal analysis. **Nor Hisam Zamakshshari:** Writing – original draft, Visualization, Software. **Sharon Hui Jiun Leong:** Methodology, Investigation, Formal analysis. **Kai Wei Yeo:** Writing – original draft. **Ainaa Nadiah Abd Halim:** Writing – review & editing, Supervision, Funding acquisition, Conceptualization.

Ethics approval and consent to participate

Not applicable.

Funding

The authors would like to thank UNIMAS under the Graduate Research Grant UNI/F07/GRADUATES/86805/2025 for providing funding to complete this work.

Data availability

The data sets used and analysed during the current study are available from the corresponding author on reasonable request.

Declaration of Competing Interest

The authors hereby declare that there is no conflict of interest with respect to the work reported in this paper.

Acknowledgement

The authors would like to acknowledge the facilities, expertise and assistance provided by the Faculty of Resources Science and Technology (FRST), Universiti Malaysia Sarawak (UNIMAS). We would also like to thank Dr Ngieng Ngui Sing and Prof. Dr Zainab Ngaini for their guidance and unwavering support.

Appendix A. Supporting information

Supplementary data associated with this article can be found in the online version at doi:10.1016/j.lddd.2026.100402.

References

1. Andrusenko I, Hamilton V, Mugnaioli E, et al. The crystal structure of orthocetamol solved by 3D electron diffraction. *Angew Chem Int Ed.* 2019;58:1–5. https://doi.org/10.1002/anie.201904564
2. Ishii H, Obara T, Kijima-Suda I. Investigation of plasma concentrations of paracetamol, metacetamol, and orthocetamol in japanese racehorses using liquid chromatography–electrospray ionisation–tandem mass spectrometry. *Drug Test Anal.* 2020;12(7):929–937. https://doi.org/10.1002/dta.2792
3. Tsemeugne J, Nangmo PK, Mkounga P, et al. Synthesis, characteristic fragmentation patterns, and antibacterial activity of new azo compounds from the coupling reaction of diazobenzothiazole ions and acetaminophen. *Heterocycl Commun.* 2021;27(1):79–89. https://doi.org/10.1515/hc-2020-0127
4. Brune K, Renner B, Tiegs G. Acetaminophen/paracetamol: a history of errors, failures and false decisions. *Eur J Pain.* 2015;19(7):953–965. https://doi.org/10.1002/ejp.621
5. Ahmed HM, Shehata HH, El-Saeed GSM, Gabal HHA, El-Daly SM. Paracetamol overdose induces acute liver injury accompanied by oxidative stress and inflammation. *Egypt J Chem.* 2023;66(3):399–408. https://doi.org/10.21608/ejchem.2022.140587.6153
6. Islam MT, Chowdhury R, Bhuia MS, et al. Antimicrobial potentials and challenges of paracetamol: a comprehensive reassessment based on database reports. *Pharm Sci Adv.* 2025;3(April):100070. https://doi.org/10.1016/j.pscia.2025.100070
7. Joolakanti HB, Kamepalli R, Miryala J, Battu S. Synthesis, docking, and biological activities of novel metacetamol embedded [1,2,3]-triazole derivatives. *J Mol Struct.* 2021;1242:130786. https://doi.org/10.1016/j.molstruc.2021.130786
8. Shinozaki T, Ono M, Higashi K, Moribe K. A novel drug-drug cocrystal of levofloxacin and metacetamol: reduced hygroscopicity and improved photostability of levofloxacin. *J Pharm Sci.* 2019;108(7):2383–2390. https://doi.org/10.1016/j.xphs.2019.02.014
9. Şenkardeş S, Atlıhan İ, Çayır E, et al. Synthesis and evaluation of novel metacetamol derivatives with hydrazone moiety as anticancer and antimicrobial agents. *Chem Biodivers.* 2023;20(8):e202300766. https://doi.org/10.1002/cbdv.202300766
10. Alkhzem AH, Woodman TJ, Blagbrough IS. Design and synthesis of hybrid compounds as novel drugs and medicines. *RSC Adv.* 2022;12(30):19470–19484. https://doi.org/10.1039/d2ra03281c
11. Santos LTD dos, Teixeira ML, Carneiro J. Synthesis of a new drug candidate trough molecular hybridization and application as a learning strategy. *Braz J Dev.* 2021;7(3):22223–22233. https://doi.org/10.34117/bjdv7n3-096
12. Tahir T, Ashfaq M, Saleem M, et al. Pyridine scaffolds, phenols and derivatives of azo moiety: Current therapeutic perspectives. *Molecules.* 2021;26(16):4872. https://doi.org/10.3390/molecules26164872
13. Ragab SS, Sweed AMK, Hamza ZK, Shaban E, El-Sayed AA. Design, synthesis, and antibacterial activity of spiropyrimidinone derivatives incorporated azo sulfonamide chromophore for polyester printing application. *Fibers Polym.* 2022;23(8):2114–2122. https://doi.org/10.1007/s12221-022-4032-4
14. Gvozdeva Y, Staynova R. pH-Dependent Drug Delivery Systems for Ulcerative Colitis Treatment. *Pharmaceutics.* 2025;17(2):226. https://doi.org/10.3390/pharmaceutics17020226
15. Gu Y, Yang R, Chen J, et al. Design and Synthesis of an Azo Reductase Responsive Flavonol–Indomethacin Hybrid Used for the Diagnosis and Treatment of Colitis. *Molecules.* 2024;29(17):4244. https://doi.org/10.3390/molecules29174244
16. Mezgebe K, Mulugeta E. Synthesis and pharmacological activities of azo dye derivatives incorporating heterocyclic scaffolds: a review. *RSC Adv.* 2022;12(40):25932–25946. https://doi.org/10.1039/D2RA04934A
17. Cerón-Carrasco JP, Jacquemin D. Using Theory To Extend the Scope of Azobenzene Drugs in Chemotherapy: Novel Combinations for a Specific Delivery. *Chem Med Chem.* 2021;16(11):1765–1775. https://doi.org/10.1002/cmdc.202100046
18. Khan MN, Parmar DK, Das D. Recent Applications of Azo Dyes: A Paradigm Shift from Medicinal Chemistry to Biomedical Sciences. *Mini-Rev Med Chem.* 2021;21(9):1071–1084. https://doi.org/10.2174/1389557520999201123210025

19. Al-Majdi ZR, Al-Dahhan WH, Shihab MS, Nazari MH. Azo Compounds and their Potential Applications: Article Review. *Al-Kitab J Pure Sci.* 2025;9(01):144–163. https://doi.org/10.32441/kjps.09.01.p10
20. Carreño A, Morales-Guevara R, Cepeda-Plaza M, et al. Synthesis, Physicochemical Characterization, and Antimicrobial Evaluation of Halogen-Substituted Non-Metal Pyridine Schiff Bases. *Molecules.* 2024;29(19):4726. https://doi.org/10.3390/molecules29194726
21. Yusuf TL, Waziri I, Oladipo SD, Abd El-Maksoud MS, Muller AJ, Vatsha B. Copper(II) Complexes Derived from Halogen-Substituted Schiff Base Ligands: Synthesis, Crystal Structures, Antibacterial Activity, and Molecular Docking Studies. *ACS Omega.* 2025;10(43):50795–50805. https://doi.org/10.1021/acsomega.4c06806
22. Zborovskii Y, Orysyk V, Orysyk S, Vovk M. Structure-Activity Relationship of Thiourea Derivatives: Influence of Substituents on Antibacterial Activity. *Lett Appl NanoBioScience.* 2025;14(3):102. https://doi.org/10.33263/lianbs143.102
23. Masih PJ, Kesharwani T, Rodriguez E, et al. Synthesis and Evaluation of 3-Halobenzo[b]thiophenes as Potential Antibacterial and Antifungal Agents. *Pharmaceuticals.* 2022;15(1):1–14. https://doi.org/10.3390/ph15010039
24. Abd Halim AN, Yeo KW, Zamakshshari NH, Phornvillay S, Ngaini Z, Diosing DN. Preparation, in vitro and in silico antioxidant and antibacterial studies of 4-aminoacetanilide azo derivatives. *J Indian Chem Soc.* 2024;101(11):101341. https://doi.org/10.1016/j.jics.2024.101341
25. Desai A, Jagdeve S, Patil N, Gadale S, Waghmode S. Microwave Assisted Synthesis of Ionic Liquids with its Applications as CO2 Capture & Antimicrobial Activity. *Res Rev Biotechnol Biosci.* 2022;9(1):2022–2023. https://doi.org/10.5281/zenodo.6619031
26. Jerwan SH, Khalaf YH, Mohammed AM. Synthesis of ZnO Nanoparticles from Azo Complexes and Study their Biological Activity. *Syst Rev Pharm.* 2021;12(1):350–358. https://doi.org/10.31838/srp.2021.1.55
27. Ahmed AI, Yousif EI. New Metal Complexes with AZO ligand; Synthesis, Spectral Characterisation and Biological Evaluation. *Pak J Med Heal Sci.* 2022;16(7):550–553. https://doi.org/10.53350/pjmhs22167550
28. Sharma S, Dhote NM, Wagh MS. Nickel Oxide Nanoparticles via Green Synthesis: Insights into Antimicrobial, Antifungal and Dye Degradation Potentials. *Int J PLANT Environ.* 2025;11(02):343–350. https://doi.org/10.18811/ijpen.v11i02.13
29. Lopez Venditti ED, Crespo Andrada KF, Bustos PS, et al. Antibacterial, Antifungal, and Antibiofilm Activities of Biogenic Zinc Nanoparticles against Pathogenic Microorganisms. *Front Cell Infect Microbiol.* 2025;15(July):1–17. https://doi.org/10.3389/fcimb.2025.1545119
30. Abd Halim AN, Mohammad Hussin AS, Ngaini Z, Zamakshshari NH, Haron IZ. Synthesis, antibacterial potential and in silico molecular docking analysis of triazene compounds via diazo coupling reactions of an amine. *Tetrahedron Lett.* 2023;132(October):154803. https://doi.org/10.1016/j.tetlet.2023.154803
31. Reed GF, Lynn F, Meade BD. Use of coefficient of variation in assessing variability of quantitative assays. *Clin Vaccin Immunol.* 2002;9(6):1235–1239. https://doi.org/10.1128/CDLI.9.6.1235-1239.2002
32. Hanwell MD, Curtis DE, Lonie DC, Vandermeersch T, Zurek E, Hutchison GR. Avogadro: an advanced semantic chemical editor, visualization, and analysis platform. *J Chemin-.* 2012;4(17):1–17. https://doi.org/10.1186/1758-2946-4-17
33. Sanner MF. Python: A programming language for software integration and development. *J Mol Graph Model.* 1999;17:57–61.
34. Eberhardt J, Santos-Martins D, Tillack AF, Forli S. AutoDock Vina 1.2.0: New Docking Methods, Expanded Force Field, and Python Bindings. *J Chem Inf Model.* 2021;61(8):3891–3898. https://doi.org/10.1021/acs.jcim.1c00203
35. Agarwal M, Afzal O, Salahuddin, et al. Design, Synthesis, ADME, and Anticancer Studies of Newer N-Aryl-5-(3,4,5-Trifluorophenyl)-1,3,4-Oxadiazol-2-Amines: An Insight into Experimental and Theoretical Investigations. *ACS Omega.* 2023;8(30):26837–26849. https://doi.org/10.1021/acsomega.3c01462
36. Alka, Gautam S, Kumari P, Khurana S, Jain P, Gupta MK. 2-((2-Mercaptobenzylidene)amino)pyridin-3-ol Schiff Base Derived Mn(II), Co(II), Ni(II), and Cu(II) Metal Chelates: Synthesis, Antimicrobial, Antioxidant, Thermo-Kinetics, Molecular Docking, and In Silico ADMET Studies. *Chem Afr.* 2025;8(8):3417–3435. https://doi.org/10.1007/s42250-025-01309-w
37. Jasim SF, Mustafa YF. Synthesis, ADME Study, and Antimicrobial Evaluation of Novel Naphthalene-Based Derivatives. *J Med Chem Sci.* 2022;5(5):793–807. https://doi.org/10.26655/jmchemsci.2022.5.14
38. Şahin İ, Çeşme M, Özgeriş FB, Tümer F. Triazole Based Novel Molecules as Potential Therapeutic agents: Synthesis, Characterization, Biological Evaluation, In-Silico ADME Profiling and Molecular Docking Studies. *Chem Biol Inter.* 2023;370(January):110312. https://doi.org/10.1016/j.cbi.2022.110312
39. Arzine A, Hadni H, Boujdi K, et al. Efficient Synthesis, Structural Characterization, Antibacterial Assessment, ADME-Tox Analysis, Molecular Docking and Molecular Dynamics Simulations of New Functionalized Isoxazoles. *Molecules.* 2024;29(14):3366. https://doi.org/10.3390/molecules29143366
40. Khaled NA, Ahmed NS, Abdelazem AZ, Mohamed NA, El-Sayed AF, Ahmed SA. Design, Synthesis, Biological Evaluation, In Silico ADME Prediction and Molecular Docking of Pyrazole-Benzamides as Multitargeting Protien Kinase Inhibitors. *J Mol Struct.* 2023;1288(September):135753. https://doi.org/10.1016/j.molstruc.2023.135753
41. Acar Çevik U, Celik I, Işık A, et al. Design, Synthesis, Molecular Modeling, DFT, ADME and Biological Evaluation Studies of Some New 1,3,4-Oxadiazole Linked Benzimidazoles as Anticancer Agents and Aromatase Inhibitors. *J Biomol Struct Dyn.* 2023;41(5):1944–1958. https://doi.org/10.1080/07391102.2022.2025906
42. Kuzminac IZ, Stevanović MZ, Jakimov DS, Sakač MN. Synthesis, Optimization, In Silico, and In Vitro Testing of D-Homo Lactone Estra-1,3,5-triene Derivatives. *Russ J Bioorg Chem.* 2024;50(3):870–881. https://doi.org/10.1134/S106816202403021X
43. Silva MP, Silva B, Costa I, et al. Domino Synthesis of a New Class of Red-Shifted and Antimicrobial Imidazole-Based Azo Dyes from 5-Aminoimidazole-4-carboxamidrazones. *Org Biomol Chem.* 2025;23(20):4983–4996. https://doi.org/10.1039/D5OB00463B
44. Benkhaya S, M'rabet S, El Harfi A. Classifications, properties, recent synthesis and applications of azo dyes. *Heliyon.* 2020;6(1) https://doi.org/10.1016/j.heliyon.2020.e03271
45. Kucha NA, Tank MJ, Pateliya RB, Malik DG. Bis Azo Disperse Dyes Derived from 2-Amino 5(4'-nitro phenyl) 1, 3, 4-thiadiazole: Synthesis and Their Multi-Functional Properties. *Int J Chem Stud.* 2024;12(6):01–08. https://doi.org/10.22271/chemi.2024.v12.i6a.12463
46. Ozkinali S, Cavus MS, Sakin B. Synthesis, structural characterization and theoretical investigations of new azo-azomethine compounds bearing acryloyl moiety. *Hittite J Sci Eng.* 2018 Dec 12;5(4):259–269. https://doi.org/10.17350/HJSE19030000101
47. Elsayed EH, Al-Wahaib D, Ali AE-D, Abd-El-Nabey BA, Elbadawy HA. Synthesis, Characterization, DNA Binding Interactions, DFT Calculations, and Covid-19 Molecular Docking of Novel Bioactive Copper(I) Complexes Developed via Unexpected Reduction of Azo-Hydrazo Ligands. *BMC Chem.* 2023;17(1):159. https://doi.org/10.1186/s13065-023-01086-y
48. Khairy T, Amin DH, Salama HM, et al. Antibacterial Activity of Green Synthesized Copper Oxide Nanoparticles against Multidrug-Resistant Bacteria. *Sci Rep.* 2024;14(1):25020. https://doi.org/10.1038/s41598-024-75147-0
49. Jiang X, Liu S, Tsona NT, et al. Matrix isolation FTIR study of hydrogen-bonded complexes of methanol with heterocyclic organic compounds. *RSC Adv.* 2017;7(5):2503–2512. https://doi.org/10.1039/C6RA26076D
50. Kowalkowska-Zedler D, Drzeżdżon J, Dołęga A, Łyszczek R, Bruździak P, Hnatejko Z, Cieśla B, Gołąbiewska A, Jacewicz D, Pladzyk A. Piperazine-Derived Heteroleptic Cd (II) Silanethiolates: Structural Insights, Catalytic Activity in Allyl Alcohol Oligomerization, and CO2 Sorption Properties. *Appl Organomet Chem.* 2025;39(9):e70336. https://doi.org/10.1002/aoc.70336
51. Adeniyi AO, Boyro DEA, Chindo IY, Mahmoud AA. Spectrophotometric and Infra-Red Analyses of Azo Reactive Dyes Derived from 2-Methyl-3-(2'-methylphenyl)-6-arylazo-4-oxoquinazoline. *Sci World J.* 2023;18(2):231–239. https://doi.org/10.4314/swj.v18i2.10
52. Viesser RV, Tormena CF. Influence of Stereoelectronic Interactions on the 13C NMR Chemical Shift in Iodine-Containing Molecules. *J Magn Reson Open.* 2022;12-13(December):100080. https://doi.org/10.1016/j.jmro.2022.100080
53. Omar AZ, El-Rahman MA, Hamed EA, El-Sadany SK, El-atawy MA. Synthesis, Spectroscopic Characterization and Dyeing Performance of Novel Bis Azo Dyes Derived from Benzidine. *Sci Rep.* 2023;13(1):7826. https://doi.org/10.1038/s41598-023-34660-4
54. Fragkiadakis M, Stergiannakos T, Charistos ND, Papadopoulos AG, Stoumpos CC, Neochoritis CG. Diving into the Shielding Surfaces: Construction of Atropisomeric Axes via Multicomponent Reactions. *Eur J Org Chem.* 2025;28(18):1–8. https://doi.org/10.1002/ejoc.202500212
55. Mohamad Fazli FJ, Jamain Z. Synthesis and Characterization of Hydrazine Bridge Cyclotriphosphazene Derivatives with Amide–Schiff Base Linkages Attached to Decyl and Hydroxy Terminal Groups. *Molbank.* 2024;2024(4):M1934. https://doi.org/10.3390/M1934

56. Andrade Breves R, Ajiola D, de Vasconcelos Vieira Lopes R, et al. Bio-Based Polyurethane Composites from Macauba Kernel Oil: Part 1, Matrix Synthesis from Glycerol-Based Polyol. *J Compos Sci.* 2024;8:363. https://doi.org/10.3390/jcs8090363
57. Abdul Rahim K, Jamain Z. Synthesis and Characterization of Amide-Based Cyclotriphosphazene Derivatives with Alkoxy Terminal Groups. *Molbank.* 2025;2025(3):M2039. https://doi.org/10.3390/M2039
58. Kara YS, Yıldız B. Synthesis and Substituent Effect Study on 13C NMR Chemical Shifts of 4-(Substitue-phenyl)-6-methyl-3-phenyl-4H-1,2,4-oxadiazin-5(6H)-one. *J Mol Struct.* 2022;1250(February):131787. https://doi.org/10.1016/j.molstruc.2021.131787
59. Yeo KW, Abd Halim AN, Zamakshshari NH, et al. Synthesis, Biological Evaluation and Molecular Docking Analysis of *p*-Tolyldiazenyl Azo Derivatives. *Malays J Anal Sci.* 2025;29(3):1331. https://doi.org/10.1002/ibra.12098
60. VH ES, Dwi Ariani SR, Wathon MH. Ultrasound-Assisted Syntheses of Some Derivatives Chalcones and Their Potential Antibacterial Activity. *Egypt J Chem.* 2025;68(11):119–128. https://doi.org/10.21608/ejchem.2025.343662.10971
61. Frickmann H, Hahn A, Berlec S, et al. On the Etiological Relevance of Escherichia coli and Staphylococcus aureus in Superficial and Deep Infections – A Hypothesis-Forming, Retrospective Assessment. *Eur J Microbiol Immunol.* 2019;9(4):124–130. https://doi.org/10.1556/1886.2019.00021
62. Rafiq K, Sani AA, Hossain MT, Hossain MT, Hadiuzzaman M, Bhuiyan MAS. Assessment of The Presence of Multidrug-Resistant Escherichia coli, Salmonella and Staphylococcus in Chicken Meat, Eggs and Faeces in Mymensingh Division of Bangladesh. *Heliyon.* 2024;10(17):e36690. https://doi.org/10.1016/j.heliyon.2024.e36690
63. Di Martino M, Sessa L, Di Matteo M, Panunzi B, Piotto S, Concilio S. Azobenzene as Antimicrobial Molecules. *Molecules.* 2022;27(17):5643. https://doi.org/10.3390/molecules27175643
64. Singh Chauhan H, Thimmaraju M, Kumar Malik J, Gupta V, Singh G. A Review on Thiadiazole-Derived Compounds: Design, Synthesis, And Antimicrobial Potential. *Int J Pharm Sci Med.* 2025;3(1):43–52. https://doi.org/10.70199/IJPSM.3.1.43-52
65. Bhandare RR, Munikrishnappa CS, Kumar GS, et al. Multistep Synthesis and Screening of Heterocyclic Tetrads Containing Furan, Pyrazoline, Thiazole and Triazole (or Oxadiazole) as Antimicrobial and Anticancer Agents. *J Saudi Chem Soc.* 2022;26(3):101447. https://doi.org/10.1016/j.jscs.2022.101447
66. Fayeulle A, Trudel E, Damiens A, et al. Antimicrobial and Antioxidant Activities of Amines Derived from Vanillin as Potential Preservatives: Impact of the Substituent Chain Length and Polarity. *Sustain Chem Pharm.* 2021;22(September):100471. https://doi.org/10.1016/j.scp.2021.100471
67. Hevey R. The Role of Fluorine in Glycomimetic Drug Design. *Chem - A Eur J.* 2021;27(7):2240–2253. https://doi.org/10.1002/chem.202003135
68. Lal J, Kaul G, Akhir A, Ansari SB, Chopra S, Reddy DN. Bio-Evaluation of Fluoro and Trifluoromethyl-Substituted Salicylanilides against Multidrug-Resistant S. aureus. *Med Chem Res.* 2021;30(12):2301–2315. https://doi.org/10.1007/s00044-021-02808-4
69. Shalo RR, Karthiga AR, Divyabharathi S, Balasankar T, Rajeswari K, Vidhyasagar T. Rational Design, Synthesis, Computational Studies and Biological Evaluation of New Diazepanone Derivatives: Crystal Structure of 2,7-Bis(4-chlorophenyl)-1,3-dimethyl-1,4-diazepan-5-one. *J Mol Struct.* 2025;1322(February):140360. https://doi.org/10.1016/j.molstruc.2024.140360
70. Adamczyk-Woźniak A, Sporzyński A. Merging Electron Deficient Boronic Centers with Electron-Withdrawing Fluorine Substituents Results in Unique Properties of Fluorinated Phenylboronic Compounds. *Molecules.* 2022;27(11):3427. https://doi.org/10.3390/molecules27113427
71. Páez-Franco JC, Zermeño-Ortega MR, de la O-Contreras CM, et al. Relevance of fluorinated ligands to the design of metallodrugs for their potential use in cancer treatment. *Pharmaceutics.* 2022;14(2):1–36. https://doi.org/10.3390/pharmaceutics14020402
72. Moreno-Narváez ME, González-Sebastián L, Colorado-Peralta R, et al. Anticancer and Antimicrobial Activity of Copper(II) Complexes with Fluorine-Functionalized Schiff Bases: A Mini-Review. *Inorganics.* 2025;13(2):38. https://doi.org/10.3390/inorganics13020038
73. Khoshbakht A, Shiran JA, Miran M, Sepehri S. Synthesis and Evaluation of In Vitro Antioxidant, Anticancer, and Antibacterial Properties of New Benzylideneiminophenylthiazole Analogues. *BMC Chem.* 2024;18(1):173. https://doi.org/10.1186/s13065-024-01273-5
74. Malik J, Karande G, Murugesan S, Sekhar KVGC. Recent advances in triazole hybrid molecules for the therapeutic management of neglected tropical diseases. *RSC Med Chem.* 2025;16(11):5292–5317. https://doi.org/10.1039/D5MD00572H
75. Muñoz KA, Hergenrother PJ. Facilitating compound entry as a means to discover antibiotics for gram-negative bacteria. *Acc Chem Res.* 2021;54(6):1322–1333. https://doi.org/10.1021/acs.accounts.0c00895
76. Tigineh GT, Sitotaw G, Workie A, Abebe A. Synthesis, characterization and in vitro antibacterial studies on mixed ligand complexes of iron(III) based on 1,10-phenanthroline. *J Korean Chem Soc.* 2021;65(3):203–208. https://doi.org/10.5012/jkcs.2021.65.3.203
77. Klobucar K, Brown ED. New potentiators of ineffective antibiotics: targeting the gram-negative outer membrane to overcome intrinsic resistance. *Curr Opin Chem Biol.* 2022;66(February):102099. https://doi.org/10.1016/j.cbpa.2021.102099
78. Zhang J, Su P, Chen H, Qiao M, Yang B, Zhao X. Impact of reactive oxygen species on cell activity and structural integrity of gram-positive and gram-negative bacteria in electrochemical disinfection system. *Chem Eng J.* 2023;451(January):138879. https://doi.org/10.1016/j.cej.2022.138879
79. Bousiakou LG, Qindeel R, Al-Dossary OM, Kalkani H. Synthesis and characterization of graphene oxide (GO) sheets for pathogen inhibition: escherichia coli, staphylococcus aureus and pseudomonas aeruginosa. *J King Saud Univ - Sci.* 2022;34(4):102002. https://doi.org/10.1016/j.jksus.2022.102002
80. Rezaeianzadeh O, Asghari S, Tajbakhsh M, Mohseni M, Khalilpour A. Synthesis, molecular docking, and anticancer evaluation of new azo-based sulfonamides against MCF-7 human breast cancer cell line. *Chem Method.* 2024;8:329–350. https://doi.org/10.48309/chemm.2024.447205.1773
81. Dzotam JK, Simo IK, Bitchagno G, et al. vitro antibacterial and antibiotic modifying activity of crude extract, fractions and 3',4',7-trihydroxyflavone from Myristica fragrans Houtt against MDR Gram-negative enteric bacteria. *BMC Complement Alter Med.* 2018;18(1):1–9. https://doi.org/10.1186/s12906-018-2084-1
82. Abd Halim AN, Ngaini Z. Synthesis and bacteriostatic activities of bis(Thiourea) derivatives with variable Chain Length. *J Chem.* 2016(1):2739832. https://doi.org/10.1155/2016/2739832
83. Greenberg M, Dodds M, Tian M. Naturally occurring phenolic antibacterial compounds show effectiveness against oral bacteria by a quantitative structure-activity relationship study. *J Agric Food Chem.* 2008;56(23):11151–11156. https://doi.org/10.1021/jf8020859
84. Lim JY, Sim KM, Teo KC. Antibacterial activity of 5-bromo substituted phenyl N -acylhydrazone derivatives with aromatic substitution at ortho- and para-directors as potential adjuvants. *BIO Web Conf.* 2025;182:02008. https://doi.org/10.1051/bioconf/202518202008
85. Demesa-castañeda AV, David JP, Hern A, Said R. Searching for new antibacterial compounds against staphylococcus aureus: a computational study on the binding between FtsZ and FtsA. *Drugs Drug Candidates.* 2024;3(4):751–773. https://doi.org/10.3390/ddc3040043
86. Blay V, Gailiunaite S, Lee CY, et al. Comparison of ATP-binding pockets and discovery of homologous recombination inhibitors. *Bioorg Med Chem.* 2022;70(April):116923. https://doi.org/10.1016/j.bmc.2022.116923
87. El-Helw EAE, Asran M, Azab ME, Helal MH, Alzahrani AYA, Ramadan SK. Synthesis and in silico studies of certain benzo[f]quinoline-based heterocycles as antitumor agents. *Sci Rep.* 2024;14(1):1–14. https://doi.org/10.1038/s41598-024-64785-z
88. Heilman DN, Hui AY, Mian VJ, et al. Unlocking the Antibacterial Potential of Xanthone from Calophyllum Species: Inhibition of Nucleic Acid Synthesis. *ChemistrySelect.* 2023;8(46):2202302737. https://doi.org/10.1002/slct.202302737
89. Du S, Pichoff S, Lutkenhaus J. FtsEX Acts on FtsA to Regulate Divisome Assembly and Activity. *Proc Natl Acad Sci.* 2016;113(34):E5052–E5061. https://doi.org/10.1073/pnas.1606656113
90. Mhaidat I, Banidomi S, Wedian F, et al. Antioxidant and Antibacterial Activities of 5-Mercapto(substitutedthio)-4-substituted-1,2,4-triazol Based on Nalidixic Acid: A Comprehensive Study on Its Synthesis, Characterization, and In Silico Evaluation. *Heliyon.* 2024;10(7):e28204. https://doi.org/10.1016/j.heliyon.2024.e28204
91. Kulandaisamy A, Panneerselvam M, Solomon RV, et al. Halogen-Based 17β-HSD1 Inhibitors: Insights from DFT, Docking, and Molecular Dynamics Simulation Studies. *Molecules.* 2022;27(12):3962. https://doi.org/10.3390/molecules27123962
92. Loose M, Mitchison TJ. The Bacterial Cell Division Proteins FtsA and FtsZ Self-Organize into Dynamic Cytoskeletal Patterns. *Nat Cell Biol.* 2013;16(1):38–46. https://doi.org/10.1038/ncb2885
93. El-Sewedy A, El-Bordany EA, Mahmoud NFH, Ali KA, Ramadan SK. One-pot Synthesis, Computational Chemical Study, Molecular Docking, Biological Study, and In Silico Prediction ADME/Pharmacokinetics Properties of 5-Substituted 1H-Tetrazole Derivatives. *Sci Rep.* 2023;13(1):17869. https://doi.org/10.1038/s41598-023-44615-4

94. Manisha, Ahmedi S, Tiwari B, Manzoor N, Kumar A, Jain P. 3d-Transition Metal Complexes of a Tridentate Ligand: Synthesis, Characterization, Physico-Chemical Studies, Antimicrobial Activity, In Silico Molecular Docking and ADME Studies. *Chem Afr.* 2025;8(5):1851–1867. https://doi.org/10.1007/s42250-025-01310-3
95. Alyar S, Alyar H, Özdemir Özmen Ü, Aktaş O, Erdem K. Biochemical Properties of Schiff Bases Derived from FDA-Approved Sulfa Drugs: Synthesis, ADME/Molecular Docking Studies, and Anticancer Activity. *J Mol Struct.* 2023;1293(December):136167. https://doi.org/10.1016/j.molstruc.2023.136167
96. Siddiqui B, Yadav CS, Ahmad A, et al. Synthesis and In-Silico Study of 5-Oxo-1, 2-diphenyl-4-(phenylamino)-2,5-dihydro-1H-pyrrole-3-carboxylate. *Afr J Biomed Res.* 2024;27(3s):4228–4233. https://doi.org/10.53555/AJBR.v27i3S.3141
97. Gökalp M, Dede B, Tilki T, Karabacak Atay Ç. Triazole Based Azo Molecules as Potential Antibacterial Agents: Synthesis, Characterization, DFT, ADME and Molecular Docking Studies. *J Mol Struct.* 2020;1212:128140. https://doi.org/10.1016/j.molstruc.2020.128140
98. Kerkour R, Moumeni O, El houda Rabhi N, et al. Synthesis, DFT Investigation, ADME-T Properties, Molecular Docking and Molecular Dynamics Simulation of New α-Aminophosphonate Inhibitor Targeting Mpro and RdRp Enzymes in SARS-CoV-2. *J Mol Struct.* 2024;1315(ember):138842. https://doi.org/10.1016/j.molstruc.2024.138842
99. Hamdi A, Yaseen M, Ewes WA, et al. Development of New Thiazolidine-2,4-dione Hybrids as Aldose Reductase Inhibitors Endowed with Antihyperglycaemic Activity: Design, Synthesis, Biological Investigations, and In Silico Insights. *J Enzym Inhib Med Chem.* 2023;38(1):2231170. https://doi.org/10.1080/14756366.2023.2231170
100. Kushwaha P, Mehrotra S, Ahmad R. Silico Screening, ADMET Analysis and Computational Simulation Studies on Garcinia indica Choisy Phytoconstituents as Prospective Antibreast Cancer Agents: A Critical Appraisal of The Neglected Plant. *3 Biotech.* 2025;15(7):201. https://doi.org/10.1007/s13205-025-04365-8
101. Islamoğlu F. Molecular Docking, Bioactivity, ADME, Toxicity Risks, and Quantum Mechanical Parameters of Some 1,2-Dihydroquinoline Derivatives were Calculated Theoretically for Investigation of Its Use as a Pharmaceutical Active Ingredient in the Treatment of Multiple. *Prospect Pharm Sci.* 2024;22(4):168–187. https://doi.org/10.56782/pps.261
102. Hussein YT, Ahmed Azeez YH. IM. In Silico Exploration of Pharmacological and Molecular Descriptor Properties of Salacinol and Its Related Analogues. *J Turk Chem Soc Sect A Chem.* 2024;11(1):279–290. https://doi.org/10.18596/jotcsa.1246781
103. Protti Í.F, Rodrigues DR, Fonseca SK, Alves RJ, de Oliveira RB, Maltarollo VG. Do Drug-Likeness Rules Apply to Oral Prodrugs? *ChemMedChem.* 2021;16(9):1446–1456. https://doi.org/10.1002/cmdc.202000805
104. Kim BH, Lee MJ, Lee WY, et al. Hair Growth Stimulation Effect of Centipeda minima Extract: Identification of Active Compounds and Anagen-Activating Signaling Pathways. *Biomolecules.* 2021;11(7):976. https://doi.org/10.3390/biom11070976
105. Ahsan R, Paul S, Alam MS, Rahman AFMM. Synthesis, Biological Properties, In Silico ADME, Molecular Docking Studies, and FMO Analysis of Chalcone Derivatives as Promising Antioxidant and Antimicrobial Agents. *ACS Omega.* 2025;10(5):4367–4387. https://doi.org/10.1021/acsomega.4c06897
106. Omran MM, Kamal MM, Ammar YA, Abusaif MS, Ismail MMF, Mansour HH. Pharmacological Investigation of New Niclosamide-Based Isatin Hybrids as Antiproliferative, Antioxidant, and Apoptosis Inducers. *Sci Rep.* 2024;14(1):19818. https://doi.org/10.1038/s41598-024-69250-5
107. Çapan İ, Gümüş M, Gökce H, Çetin H, Sert Y, Koca İ. Synthesis, Dielectric Properties, Molecular Docking and ADME Studies of Pyrrole-3-ones. *J Biomol Struct Dyn.* 2022;40(19):8655–8671. https://doi.org/10.1080/07391102.2021.1914174
108. Boutiddar R, Abbiche K, Baammi S, El Hammadi A, Mogren Al Mogren M, Hochlaf M. Silico Structural Study, Design and Efficacy Evaluation of Fluoro Isoxazolidine Derivatives as Potential Antibacterial Agents. *J Fluor.* 2025;35(10):10381–10399. https://doi.org/10.1007/s10895-025-04302-1
109. Domínguez-Villa FX, Durán-Iturbide NA, Ávila-Zárraga JG. Synthesis, Molecular Docking, and In Silico ADME/Tox Profiling Studies of New 1-Aryl-5-(3-azidopropyl)indol-4-ones: Potential Inhibitors of SARS CoV-2 Main Protease. *Bioorg Chem.* 2021;106(January):104497. https://doi.org/10.1016/j.bioorg.2020.104497
110. Al-Hujaj HH, Majed AA, Abdalzahra QR, et al. Thiazolidine derivatives as promising prostate cancer agents: design, synthesis, in vitro evaluation, DFT, ADME, POM, Docking, and Toxicity Studies. *J Mol Struct.* 2025;1340(September):142544. https://doi.org/10.1016/j.molstruc.2025.142544